SEL-65-063

Eccentric Geophysical-Observatory Satellite S-49 with Interpretation of the Radio-Beacon Experiment

by

A.V. da Rosa

June 1965

Technical Report No. 1

Prepared under
National Aeronautics and Space Administration
Contract NASR-136

RADIOSCIENCE LABORATORY

STANFORD ELECTRONICS LABORATORIES

STANFORD UNIVERSITY • STANFORD, CALIFORNIA

SEL-65-063

ECCENTRIC GEOPHYSICAL-OBSERVATORY SATELLITE S-49 WITH INTERPRETATION OF THE RADIO-BEACON EXPERIMENT

by

A. V. da Rosa

June 1965

Technical Report No. 1

Prepared under
National Aeronautics and Space Administration Contract NASR-136

Radioscience Laboratory
Stanford Electronics Laboratories
Stanford University Stanford, California

ABSTRACT

12993

The S-49 satellite, launched on 5 September 1964, carried a pair of radio beacons operating at harmonically related frequencies modulated by 20- and 200-kc signals. The radio-beacon experiment was designed to investigate the exosphere by studying the behavior of the columnar electron content between ground and satellite as the latter moves from perigee to apogee in its highly eccentric orbit. To avoid errors arising from over-simplified assumptions about the dense ionosphere, which would mask the effects in the exosphere, simultaneous measurements were made of the differential-Doppler frequency and the Faraday-rotation angle. The former provides columnar-content information from ground to transmitter while the latter yields columnar-content information determined mainly by the ionization in the lower ionosphere. The difference between the contents thus obtained can be attributed to the columnar content of the exosphere up to satellite height and should be essentially independent of variations in the lower ionosphere.

The objective of the present report is to describe the underlying principles and the techniques for translating the rad data received from the EGO beacon experiment into curves of slant columnar content in the exosphere vs time. These curves are the starting point for an analysis of the exospheric behavior. Such an analysis, however, is not a part of the present report.

The usual first-order analysis of the differential-Doppler-frequency and the Faraday-rotation-angle data is complicated in the present case by the rotation of the satellite antenna. The effect of this rotation is investigated and methods for taking it into account are developed. The effects of various approximations usually made in the first-order analysis are investigated and, when necessary, proper corrections are introduced.

In brief, the use of this report will permit the specification of scaling techniques for the records bearing the raw data from the satellite and the writing of computer programs that will yield exospheric columnar contents.

Author

CONTENTS

ILLUSTRATIONS

SYMBOLS

c	velocity of light, 3×10^8 m/sec
ds	path element
E	electric field intensity, volts/m
e	base of natural logarithms; also charge of the electron, mks
f	a general frequency, cps
f_D	differential-Doppler beat frequency
f_M	modulation frequency
G	mean value of product H cos θ
H	geomagnetic field intensity, ampere-turns/m
H	scale height of Chapman layer m
I	total electron content (vertical), electrons/m^2
I_S	total electron content (slant), electrons/m^2
I_{SD}	total electron content (slant), from differential-Doppler frequency, electrons/m^2
I_{SD_o}	reference value of I_{SD}, electrons/m^2
I_{SF}	total electron content (slant), from Faraday-rotation angle, electrons/m^2
K_D	a constant, 80.62 m^3/sec^2
K_F	a constant, 0.02976, mks
m	mass of the electron, kg
N	electron concentration, electrons/m^3
n	ratio between higher and lower frequency of differential-Doppler pair
P	apparent spin period of satellite, sec
P	phase path length, m
P_o	true spin period of satellite, sec

Q	a constant relating the time derivative of the total slant content to the differential-Doppler frequency, 3.31×10^{-15}, mks
R	path length, m
s	length along the path, m
t	time, sec
v_p	phase velocity, m/sec
v_g	group velocity, m/sec
X	ω_p^2/ω^2
$\overline{X}$	height average of X
Y	ω_g/ω
Y	plane defined by antenna firing axis at position of observer
Y_o	Y plane at initial time
Y_L	$\pm (\omega_g/\omega)\cos\theta$ (negative sign for electrons)
Y_T	$\pm (\omega_g/\omega)\sin\theta$ (negative sign for electrons)
ΔP	Phase-path difference between a wave in vacuum and one in an ionized medium, both having the same terminal points, m
α	angle between the firing axis and the spin axis of the satellite antenna
ϵ	permittivity of medium
ϵ_o	permittivity of free space
ζ	angle between line of sight and spin axis of satellite antenna
θ	angle between ray path and direction of geomagnetic field, radians
λ	a general wavelength, m
μ	phase refractive index
μ	group refractive index
Υ	angle between planes Y_o and Y, radians
ϕ	a general phase angle, radians

SYMBOLS (Cont)

ϕ_r	a phase angle at the input of a receiver, radians
χ	zenithal angle of the line of sight from source to observer, radians
ψ	angle of polarization of the transmitted electric vector, radians
Ω	Faraday-rotation angle, radians
ω	a general angular frequency, radians/sec
ω_D	$2\pi f_D$
ω_g	electron gyro frequency
ω_p	electron plasma frequency
ω_r	a frequency at the input of a receiver
ω_l	angular spin frequency of satellite antenna

ACKNOWLEDGMENTS

The guidance of Professor O. K. Garriott and valuable discussions with Mr. Robert Lawrence are gratefully acknowledged.

The author wishes to thank the assistance of Mr. Stanley C. Hall in gathering the data for this work and that of Mrs. Ulla Lundquist in the scaling of the records.

The work was financed by Contract NASR-136 with the National Aeronautics and Space Administration.

I. INTRODUCTION

Measurement of the columnar content of the ionosphere by means of satellites is, by now, a well-established tool for the study of the ionized layers of the earth's atmosphere. Diurnal, seasonal, and solar-cycle variations in these layers have been analyzed. Continuous monitoring of the columnar content through the use of geostationary satellites is yielding richly detailed additional information on diurnal variations, and the characteristics of observed irregularities have been measured. Latitude dependence of the ionization has also been an objective of research by this method.

The present report describes the techniques used to extend satellite measurements of columnar content to the investigation of the exosphere.

II. THE SATELLITE

The S-49 satellite, also known as EGO (Eccentric Geophysical Observatory) or OGO-A, was launched on 5 September 1964 and carries aboard, among other experiments, a pair of radio beacons operating at harmonically related frequencies (40.01 and 360.09 Mc), which are modulated by 20- and 200-kc signals. The various spectral components have the output powers shown below.

Frequency (Mc)		Output Power (mw)
40	Carrier	230
	Each 200-kc sideband	230
	Each 20-kc sideband	55
360	Carrier	125
	Each 200-kc sideband	20
	Each 20-kc sideband	12.5

The 40-Mc transmitting antenna is a simple dipole (gain: 2 db); the 360-Mc antenna is a yagi (gain: 8 db). The orbit of the satellite is highly eccentric: apogee is at nearly 149,000 km, while perigee (which occurs at about 20° S geographic latitude) has been steadily increasing in height, at a rate of some 5,000 km/year. On 28 February 1965, it was at slightly more than 3,000-km altitude. The period of the orbit is very nearly 64 hours. The inclination of the orbit, unlike that of less-eccentric satellites, is also growing. The rate is about 18 deg/year; at the above date, it had reached a value of 39.1 deg.

It was planned to have an earth-stabilized satellite, but difficulties that appeared immediately after launch caused the satellite to spin at a rate of 5 rpm, introducing some unexpected complications in the radio-beacon experiment. The spin-axis orientation is not known precisely. Values of 42.5 deg in right ascension and -9 deg in declination, suggested by some independent measurements, were used in interpreting the data.

Figure 1 shows the general configuration of the satellite.

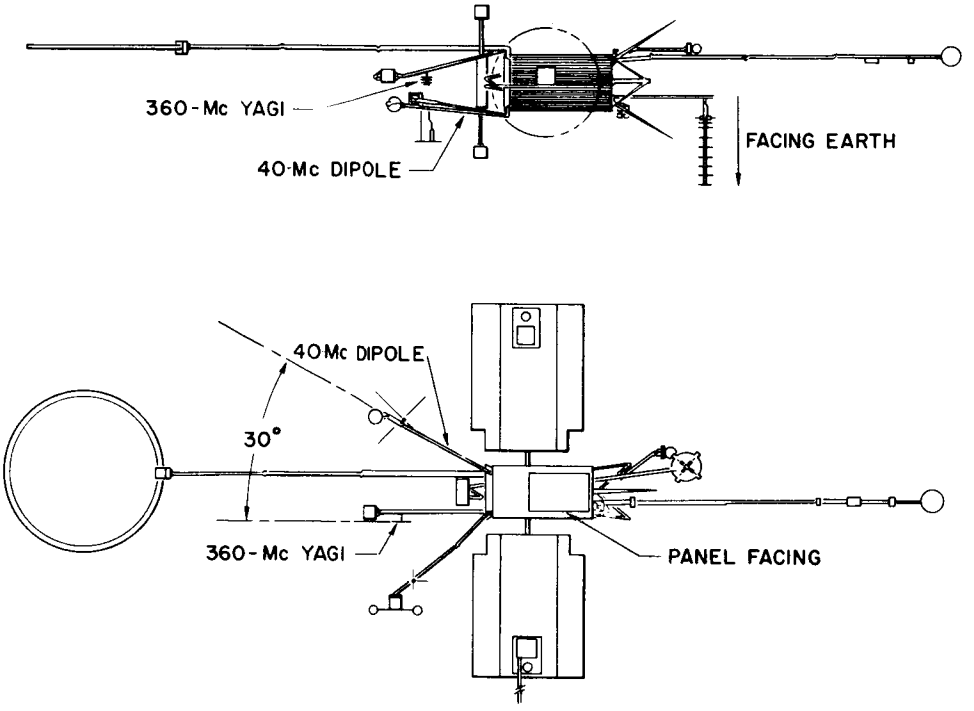

FIG. 1. GENERAL CONFIGURATION OF THE EGO, SHOWING THE POSITIONS OF THE TWO RADIO-BEACON ANTENNAS.

III. GENERAL DISCUSSION OF THE ANALYSIS

The radio-beacon experiment aboard the EGO satellite was designed with the objective of investigating the exosphere by studying the behavior of the columnar electron content between ground and satellite as the latter rises from perigee in its very eccentric orbit. Since this involves looking at a tenuous exosphere through a much denser ionosphere, it became immediately apparent that simple assumptions about the latter, such as time invariance and horizontal stratification, would lead to errors that would completely mask the effects sought. To avoid this difficulty, it was decided to make simultaneous measurements of the differential-Doppler frequency and the Faraday-rotation angle. The former can be translated into columnar content from ground to transmitter while the latter, being weighted by the geomagnetic field, yields columnar content determined mainly by the ionization below, say, 1000 km. The difference between the contents thus obtained can be attributed to the columnar content of the exosphere up to satellite height and should be fairly independent of the variations in the lower ionosphere.

Both the differential-Doppler-frequency and the Faraday-rotation-angle methods require independent measurement of an absolute reference value--in the Doppler method because of an unknown integration constant and in Faraday method because of the uncertainty in the number of half rotations.

The absolute reference for Doppler is derived from group-delay measurements and, as can be seen in Fig. 2, there is a good agreement between the shapes of the columnar-content-vs-time curves obtained by the two methods. Unfortunately, instrumentation difficulties have caused us to place little reliance on the absolute values thus obtained. It appears, however, that there is no fundamental difficulty in the method and it can probably be made to yield useful results. Many conclusions can be drawn from the EGO radio-beacon data even when these absolute values are unknown, because they do not affect the shape of the columnar-content-vs-time curve.

The measurement of the absolute reference level for the Faraday-rotation-angle columnar-content curve is more critical because here the slope of the curve is dependent on the level, which is derived from the

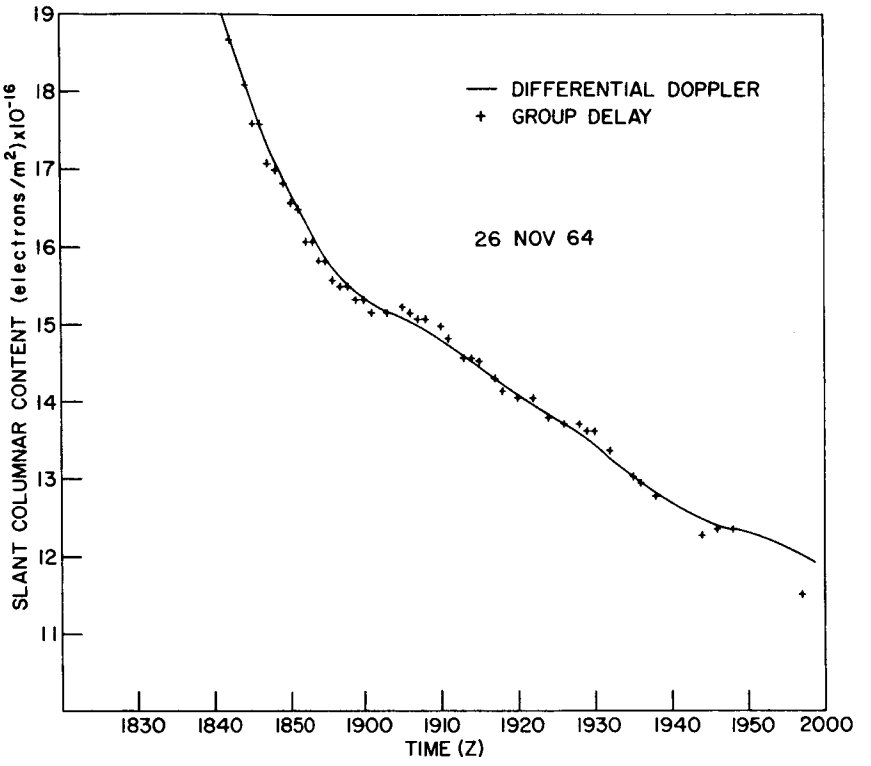

FIG. 2. COLUMNAR CONTENT VS TIME, DERIVED FROM GROUP-DELAY MEASUREMENTS. Shape of curve, in general, shows good agreement with results obtained from differential-Doppler-frequency data.

differential-Faraday-rotation angle between the two 200-kc sidebands of the 40-Mc signal. This latter measurement leads to a wide scatter of points (Fig. 3) but, with suitable averaging process, it is believed that errors of less than ±10 percent can be attained. Our confidence in this accuracy is bolstered by comparisons with simultaneous measurements made with Syncom III and S-66 satellites [Garriott, Smith and Yuen, 1965].

Curves of columnar density vs time are shown in Fig. 4. The Doppler and Faraday results are obtained independently, and it can be seen that the irregularities in the ionosphere are faithfully reproduced in both traces. For the present investigation, it is the difference between the two slant-content curves that is of interest. Figure 5 shows this difference for the three days represented in Fig. 4. Because of the difficulties mentioned before with the group-delay measurements, it was impossible to assign a correct value to the magnitude of the difference;

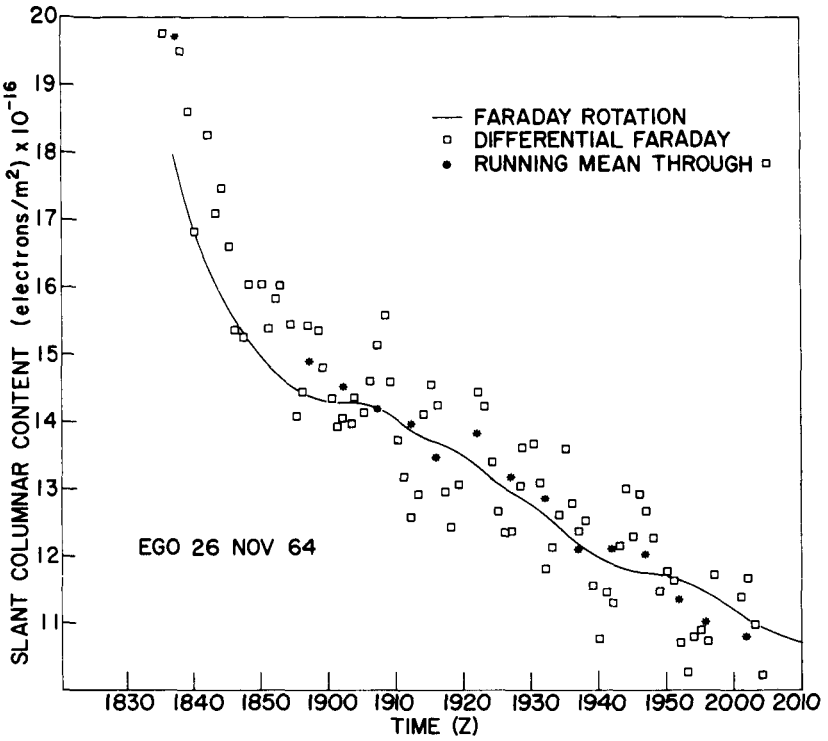

FIG. 3. COLUMNAR CONTENT VS TIME, DERIVED FROM DIFFERENTIAL-FARADAY MEASUREMENTS, SHOWING WIDE SCATTER DUE TO SCALING DIFFICULTIES. Asterisks represent values of running mean through measured points.

the shape of the curve vs height or time, however, gives useful information.

Figure 6 shows reproductions of two stretches of the graphic-recorder charts that consitute the raw data used. It can be seen that, under certain conditions, the differential-Doppler beat note has a very distorted shape, which can introduce considerable difficulties in the scaling. The cause of this distortion is explained in Chapter IV.

The amplitude fluctuations of the 360-Mc carrier, being relatively unaffected by the Faraday effect, are used to measure the spin rate of the satellite. The differential-Faraday data are obtained by scaling the time difference between the lower- and upper-sideband minima and comparing this with the period between two consecutive minima of one of the sidebands.

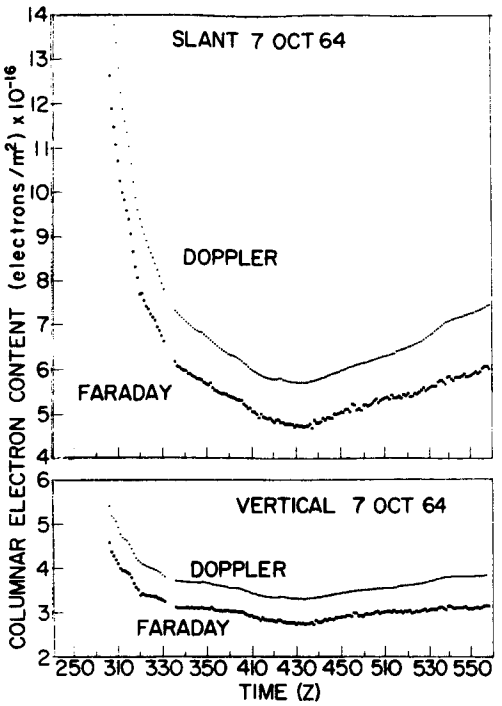

a. Early morning

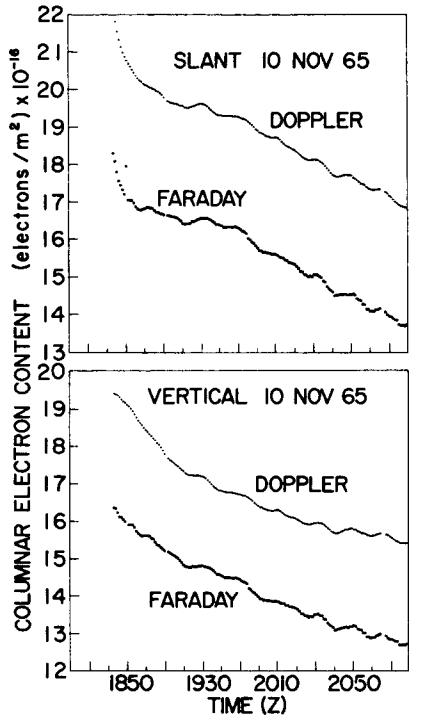

b. Midday

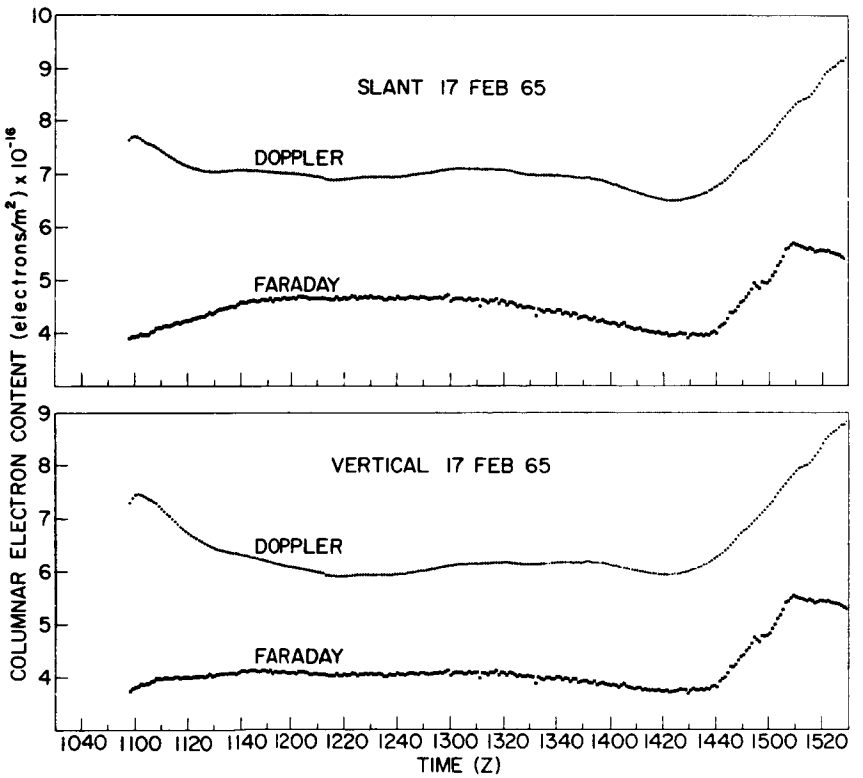

c. Early evening

FIG. 4. COLUMNAR ELECTRON CONTENT VS TIME, SHOWING BOTH DOPPLER AND FARADAY RESULTS. Sunset and sunrise effects are clearly visible in the beginning of the vertical-content curves for a. and c., respectively. Ionospheric irregularities, more prevalent during the day, can be seen in b. Nighttime ionization in this phase of the sunspot cycle seems to be quite steady.

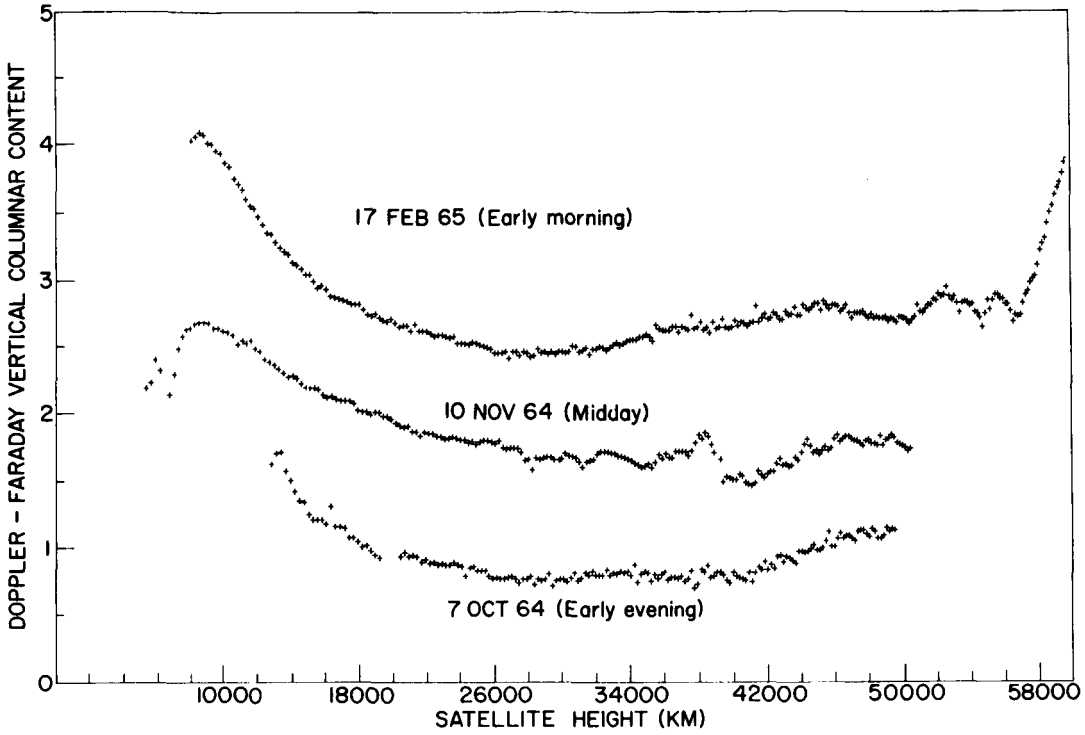

FIG. 5. DIFFERENCE BETWEEN SLANT COLUMNAR DENSITIES OBTAINED FROM DOPPLER AND FARADAY MEASUREMENTS ON THREE REPRESENTATIVE DAYS SHOWN IN FIG. 4.

The Faraday-rotation angle is obtained by scaling the time of occurrence of a minimum to the nearest 0.1 sec, and comparing the interval between two minima with the spin period of the satellite. The differential-Doppler frequency is scaled by a simple cycle count. Group-delay data are collected by annotating the phase-meter readings. In general, all data were scaled at 1-min intervals.

In view of the fact that our interest lies in observing the small difference between two large columnar-content values, it became important to examine critically all approximations made. Several corrections had to be introduced into the first-order theory, which is briefly reviewed in Chapter VII. The approximations and corrections mentioned are dealt with in subsequent chapters.

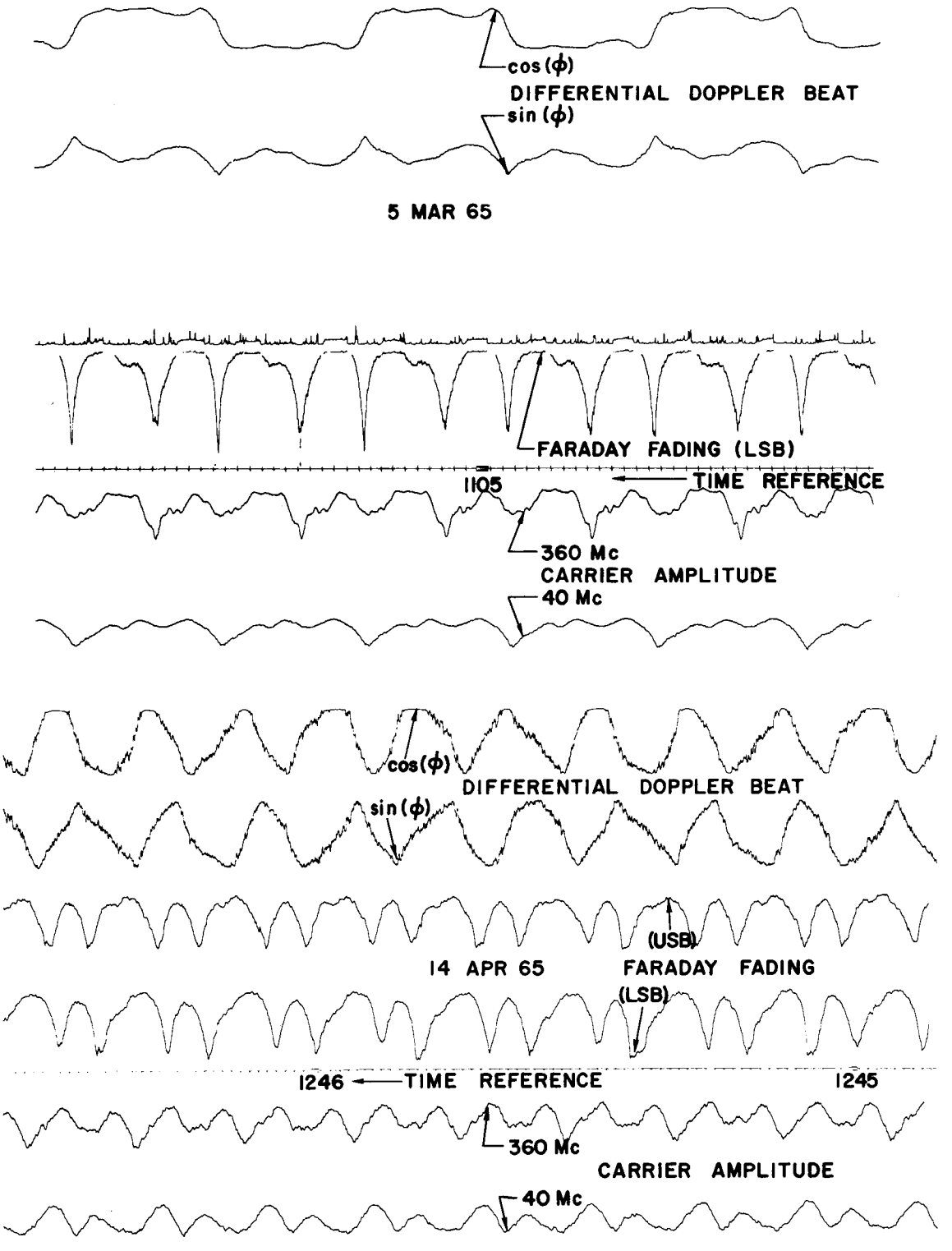

FIG. 6. EXAMPLES OF GRAPHIC-RECORDER CHARTS CONTAINING THE RAW DATA USED IN THIS STUDY.

IV. SIGNALS RECEIVED FROM A SPINNING ANTENNA

A. GENERAL

The EGO was designed to be stabilized and earth-oriented. Unfortunately, this objective was not achieved and the ground observer receives a signal radiated from a spinning, linearly polarized antenna whose firing axis (defined in Section B) is not parallel to the spin axis. In addition, the antenna is seen under continuously varying aspect angle as the satellite moves in its orbit.

This unexpected motion causes not only an amplitude modulation due to the wobbling of the radiation pattern but also results in the addition of the spin frequency to (or the subtraction of it from) the radiated frequency when the receiving antenna is circularly polarized. The 40- and 360-Mc signals are thus no longer in strict harmonic relationship, and a beat note appears in the combined output of the two differential-Doppler receivers. This effect has to be taken into account when interpreting the data.

B. DIFFERENTIAL-DOPPLER BEAT FREQUENCY

Define the firing axis of an antenna as any chosen line in the equatorial plane of a dipole or the line in the equatorial plane of a yagi corresponding to the direction of maximum radiation. Consider a linearly polarized antenna, spinning around an axis that makes an angle α with the firing axis, as in Fig. 7.

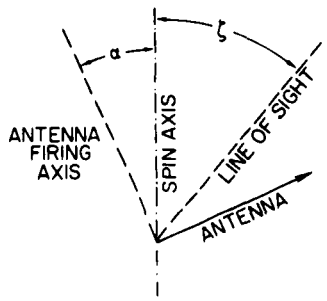

FIG. 7. ANGLES BETWEEN ANTENNA FIRING AXIS, LINE OF SIGHT, AND SPIN AXIS.

As seen by an observer whose line of sight makes an angle ζ with the spin axis, one extremity of the antenna appears to describe an ellipse, as shown in Fig. 8.

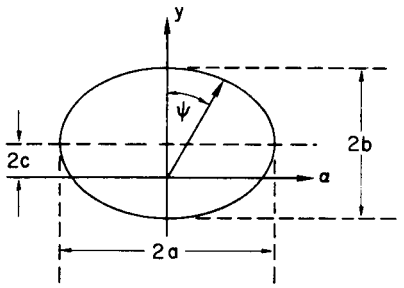

FIG. 8. GENERAL ELLIPSE DESCRIBED BY THE EXTREMITY OF THE ANTENNA AS SEEN FROM THE OBSERVER'S POSITION.

If we assume that the radiation pattern of the antenna is that shown in Fig. 9, then it can be shown that the field strength is proportional to the apparent length of the antenna projected on a plane perpendicular to the line of sight and that, in consequence, Fig. 13 also represents the field strength E near the receiver.

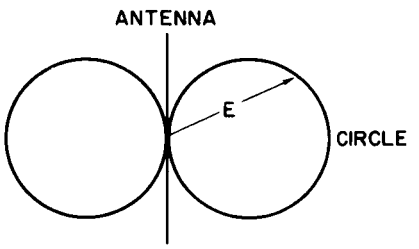

FIG. 9. ASSUMED ANTENNA RADIATION PATTERN.

The geometry indicated in Fig. 10 allows us to relate the parameters b and c of the ellipse to the angles α and ζ. The value of a can be taken as a reference scale factor.

$$2c = a \sin \zeta \tan \alpha$$

$$b = a \cos \zeta .$$

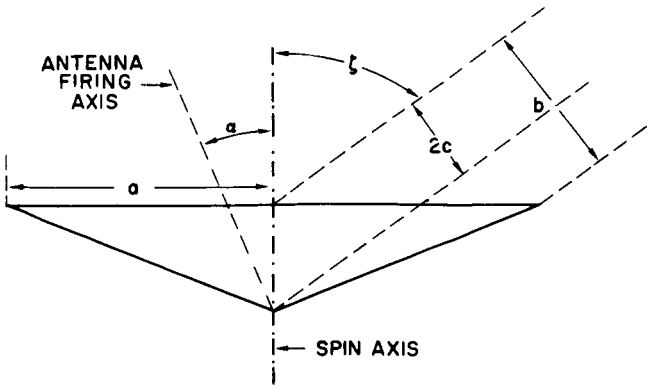

FIG. 10. SIDE VIEW OF CONE DESCRIBED BY A SPINNING ANTENNA WHOSE FIRING AXIS MAKES AN ANGLE α WITH THE SPIN AXIS.

Let ω be the angular frequency of the radiated signal and ω_1 the angular spin frequency of the antenna. The rotating vector in Fig. 8 represents a linearly polarized electric field with components

$$E_x = 2a \sin \omega_1 t \cos \omega t \tag{1a}$$

$$E_Y = 2(c + b \cos \omega_1 t) \cos \omega t \tag{1b}$$

and pointing in a direction

$$\psi = \arctan \frac{a \sin \omega_1 t}{c + b \cos \omega_1 t} .$$

Equation (1) can be rewritten as

$$E_x = a \sin(\omega+\omega_1)t - a \sin(\omega-\omega_1)t \equiv E_{x_R} + E_{x_L} \tag{2a}$$

and

$$E_y = [c \cos \omega t + b \cos(\omega+\omega_1)t] + [c \cos \omega t + b \cos(\omega-\omega_1)t]$$

$$\equiv E_{y_R} + E_{y_L} \tag{2b}$$

so that $\vec{E} \equiv \vec{E}_R + \vec{E}_L$.

Assume now that we have a circularly polarized receiving antenna consisting of two orthogonal linear elements, one oriented along the x and one along the y direction, and connected in such a way that the y-element voltage is retarded a quarter period $(\pi/2\omega)$. Such an antenna is right circularly polarized. The output voltage is the sum of the voltages from each element.

$$E = E_{x_R}(t) + E_{y_R}\left(t - \frac{\pi}{2\omega}\right) + E_{x_L}(t) + E_{y_L}\left(t - \frac{\pi}{2\omega}\right)$$

$$= a \sin(\omega+\omega_1)t + c \cos \omega\left(t - \frac{\pi}{2\omega}\right) + b \cos\left[\left(\omega+\omega_1\right)\left(t - \frac{\pi}{2\omega}\right)\right] - a \sin(\omega-\omega_1)t$$

$$+ c \cos \omega\left(t - \frac{\pi}{2\omega}\right) + b \cos\left[\left(\omega-\omega_1\right)\left(t - \frac{\pi}{2\omega}\right)\right]$$

$$= a \sin(\omega+\omega_1)t + c \sin \omega t + b \cos\left(\omega t - \frac{\pi}{2} + \omega_1 t - \frac{\pi}{2}\frac{\omega_1}{\omega}\right) - a \sin(\omega-\omega_1)t$$

$$+ c \sin \omega t + b \cos\left(\omega t - \frac{\pi}{2} - \omega t + \frac{\pi}{2}\frac{\omega_1}{\omega}\right).$$

But $\omega_1 \ll \omega$; hence the term $(\pi/2)(\omega_1/\omega)$ can be dropped:

$$E = a \sin(\omega+\omega_1)t + b \cos\left[\left(\omega t - \frac{\pi}{2}\right) + \omega_1 t\right] + 2c \sin \omega t - a \sin(\omega-\omega_1)t$$

$$+ b \cos\left[\left(\omega t - \frac{\pi}{2}\right) - \omega_1 t\right]$$

$$= a \sin(\omega+\omega_1)t + b \sin \omega t \cos \omega_1 t + b \cos \omega t \sin \omega_1 t + 2c \sin \omega t$$

$$- a \sin(\omega-\omega_1)t + b \sin \omega t \cos \omega_1 t - b \cos \omega t \sin \omega_1 t$$

$$= a \sin(\omega+\omega_1)t + b \sin(\omega+\omega_1)t + 2c \sin \omega t - a \sin(\omega-\omega_1)t + b \sin(\omega-\omega_1)t$$

$$= (b+a) \sin(\omega+\omega_1)t + (b-a) \sin(\omega-\omega_1)t + 2c \sin \omega t . \qquad (3)$$

We observe that, when $c = 0$ and $a = b$ (i.e., when we are looking down the spin axis) then the receiving antenna described above receives only the E_R component because the radiation can be split into two

circular components. When $a \neq b$ and $c \neq 0$, there are <u>three</u> frequencies present, namely, $\omega-\omega_1$, ω, and $\omega+\omega_1$.

When seen perpendicularly to the spin axis, the first and third frequencies are associated with signals of identical amplitude. At other view angles, one of these will predominate, while the signal with frequency ω is always small.

In the case of the EGO, the spin frequency is approximately 1/12 cps. The loop filter of most phase-lock receivers will accept a band of more than 10 cps. It is therefore clear that the VCO will lock on the combined signal, assuming an average frequency equal to that of the most intense of the three components while the remaining two will phase-modulate the output.

This fact can be visualized if Eq. (3) is represented by phasors plotted on a frame rotating with an angular speed equal to the angular frequency of the dominant component.

Let the amplitude of phasor AB = a+b, that of BC = a-b, and that of CD = 2c.

If $a > 0$, then the dominant component has frequency $\omega+\omega_1$ and the VCO will have a phase $(\omega+\omega_1)t+\phi_{CW}$, where ϕ_{CW} can be determined by studying Fig. 11.

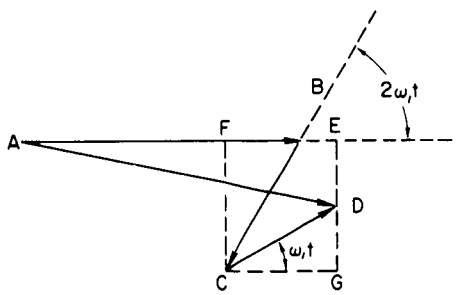

FIG. 11. PHASORS REPRESENTING EQ. (3). The VCO will have the same average frequency as that of phasor AB but will be phase-modulated by ϕ.

$$AE = AB - BF + FE = (b+a) + (b-a)\cos 2\omega_1 t + 2c \cos \omega_1 t$$

$$DE = -FC + DG = (b-a)\sin 2\omega_1 t + 2c \sin \omega_1 t$$

$$\tan \phi_{CW} = \frac{DE}{AE} = \frac{(b-a)\sin 2\omega_1 t + 2c \sin \omega_1 t}{(b+a) + (b-a)\cos 2\omega_1 t + 2c \cos \omega_1 t} . \qquad (4a)$$

If the spin is counterclockwise, then the VCO will have a phase $(\omega-\omega_1)t+\phi_{CCW}$,

$$\tan \phi_{CCW} = \frac{-(b+a) \sin 2\omega_1 t - 2c \sin \omega_1 t}{(b-a) + (b+a) \cos 2\omega_1 t + 2c \cos \omega_1 t} \qquad (4b)$$

and $a < 0$.

Since two harmonically related frequencies ω and $n\omega$ $(n = 9)$ are transmitted, the phases of the VCO's of the two receivers on the ground will be

$$(\omega + \omega_1)t + \phi \qquad \text{and} \qquad \left(\omega + \frac{\omega_1}{n}\right)t + \frac{\phi}{n} ,$$

respectively. (The higher-frequency receiver has its VCO effectively locked at $1/n$ times the incoming frequency.)

The phase comparator will see the difference

$$\phi_{diff} = \omega_1\left(1 - \frac{1}{n}\right) t + \phi\left(1 - \frac{1}{n}\right)$$

or

$$\phi_{diff} = \frac{8}{9}(\phi_{CW} + \omega_1 t) .$$

If the spin direction were reversed, then we would have

$$\phi_{diff} = \frac{8}{9}(\phi_{CCW} - \omega_1 t) .$$

Finally, if one of the receiving antennas is left and the other right circular, then the phase difference will be

$$\phi_{diff} = \frac{10}{9}(0 \pm \omega_1 t) .$$

In conclusion, the spinning antenna on the satellite causes a beat note to appear in the output of the phase comparator. The frequency of this beat (which must be removed in order to recover the ionization

effects) can be either 8/9 or 10/9 the spin frequency, depending on the relative polarization of the 40- and 360-Mc antennas on the ground. The beat is not sinusoidal, being distorted by the phase modulation as a result of the time dependence of ϕ.

When the view angle ζ is small, the distortion is insignificant. As ζ increases, ϕ becomes more significant and, as 90 deg is approached, wild deformations in the wave shape appear, making it nearly impossible to scale accurately.

This fact is illustrated in Fig. 12, which shows the computer-synthesized waveforms representing $\sin \phi_{diff}$ for $\alpha = 7.5$ deg, an 8/9 coefficient, and various values of ζ. These may be compared with the waveforms in Fig. 6.

C. PHASE MODULATION RESULTING FROM SEPARATION OF SATELLITE ANTENNAS

Because the firing axes of the 40- and 360-Mc antennas are not collinear, there should be a phase modulation in exactly the same rhythm as the rotation rate, except when we observe the satellite exactly along the spin axis. Such a phase modulation is also responsible for the considerable distortion of the waveforms. The pertinent geometry is displayed in Fig. 13. The rotation of the vehicle causes the relative distances of the two antennas to the observer to vary cyclically, so that the received phase ϕ_0 (in the absence of radial motion or ionospheric variations) is

$$\phi_{0_{40}}(t) = \phi_{40}(0) + \omega_{40}t + \frac{2\pi}{\lambda_{40}} 2b \sin \zeta \sin \omega_1 t \pm \omega_1 t$$

and

$$\phi_{0_{360}}(t) = \phi_{360}(0) + 9\omega_{40}t - \frac{2\pi}{\lambda_{360}} 2\alpha \sin \zeta \sin \omega_1 t \pm \omega_1 t ,$$

where: ω_{40} is the angular frequency fed to the 40-Mc antenna; λ represents the wavelengths associated with the two radiated carriers; a, b, and ζ are self-evident from Fig. 13; and ω_1 is the angular spin frequency. Neglecting the initial phases, which are unimportant, we

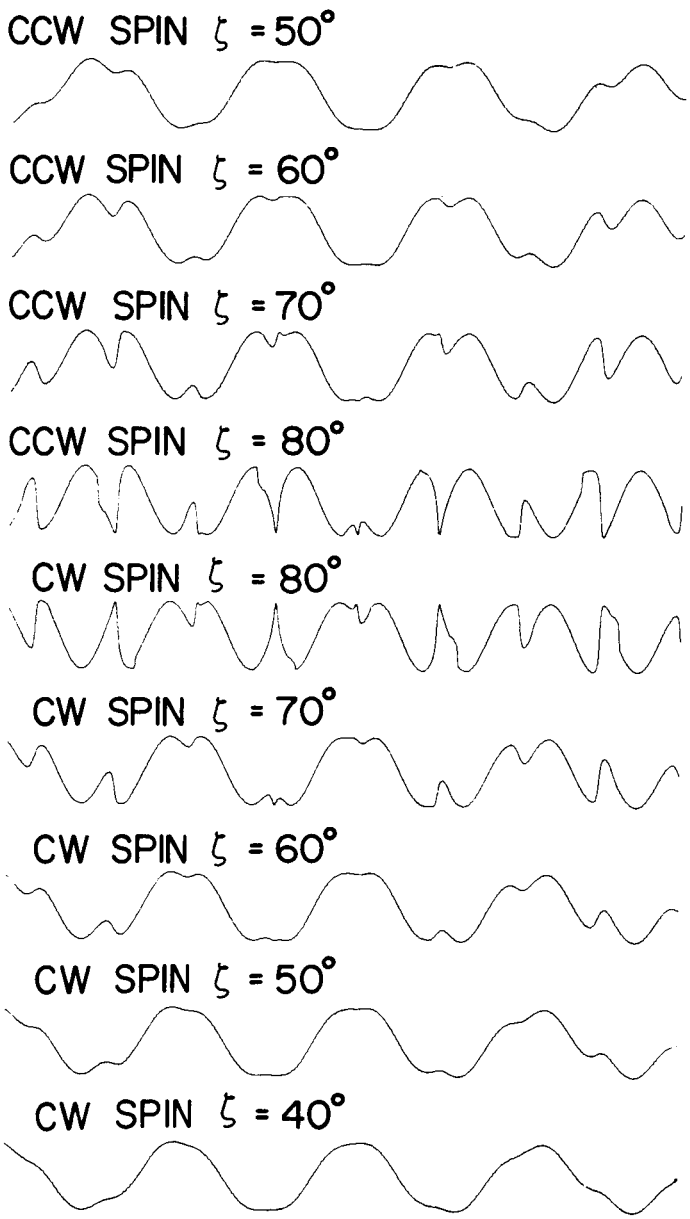

FIG. 12. WAVEFORMS SYNTHESIZED BY A DIGITAL COMPUTER REPRESENTING THE OUTPUT OF THE PHASE COMPARATOR OF A DIFFERENTIAL-DOPPLER RECEIVING SYSTEM TUNED TO A SIGNAL RADIATED FROM TWO SPINNING DIPOLES. Angle between spin and firing axes was 7.5 deg, and different values of view angle ζ are shown. Both receiving antennas were taken as right circular. One can observe the large distortions that appear when ζ approaches 90 deg.

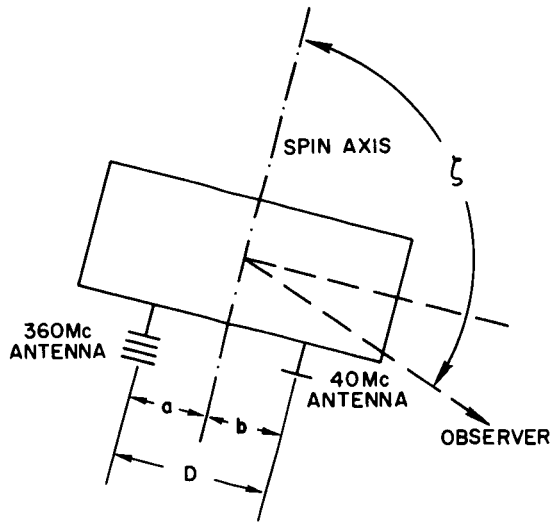

FIG. 13. SCHEMATIC REPRESENTATION OF EGO SHOWING THE DIFFERENT QUANTITIES NECESSARY TO CALCULATE THE PHASE MODULATION RESULTING FROM THE SEPARATION OF THE 40- AND 360-MC ANTENNAS.

obtain for the phase of the differential-Doppler beat,

$$\phi_D = \frac{2\pi}{\lambda_{40}} 2b \sin\zeta \sin\omega_1 t \pm \omega_1 t + \frac{2\pi}{9\lambda_{360}} 2\alpha \sin\zeta \sin\omega_1 t \pm \frac{\omega_1 t}{9}$$

$$= \frac{2\pi}{\lambda_{40}} 2(a+b) \sin\zeta \sin\omega_1 t + A\omega_1 t$$

or

$$\phi_D = \frac{4\pi}{7.5} D \sin\zeta \sin\omega_1 t + A\omega_1 t ,$$

where A can assume one of the four values (8/9, -8/9, 10/9, -10/9) as discussed in the previous section.

When this additional phase modulation is taken into account, the waveforms of the output of the phase comparators suffer a further distortion.

Changes in ionization in the raypath would result in a frequency f_D in the output of the phase comparator if the satellite did not spin. To obtain f_D from the observed frequency f_r, one applies the equation $f_D = f_r + Af_1$, where A is ±8/9 or ±10/9 depending on antenna polarization and satellite spin direction, and f is the apparent spin frequency of the satellite, as discussed in Section A.

It proves convenient to use antennas for 40 and 360 Mc of opposite polarization. This use gives a larger offset and less chances of reversal in the sign of f_D during a run, which might make the scaling more difficult. In addition, it turns out that second-order corrections are much smaller, in the Northern Hemisphere, when the 40-Mc antenna is left-polarized [Ross, 1965]. This fact leads us to prefer the left-circular antenna for 40 Mc and the right-circular for 360 Mc.

V. APPARENT SPIN RATE OF THE SATELLITE

In the calculation of the total electron content from both the Doppler and the Faraday data, knowledge of the exact spin rate of the satellite is a critical factor.

Although eddy-current losses and other phenomena tend to reduce the spin rate progressively, the effect is small enough so as to be negligible during any particular pass. On the other hand, certain mechanical maneuvers on the satellite, such as slewing the solar panels, introduce changes in the spin that cannot be predicted. Fortunately, such maneuvers are infrequent.

What must be taken into account in the data reduction is the apparent variation in spin rate that results from the relative motion of observer and satellite.

Assume that the spin axis of the satellite is parallel to the firing axis of the antenna, and consider a plane Y defined by this firing axis and the position of the observer. Let Y_0 be a plane that coincides with Y at $t = 0$ and is fixed in a frame that moves with the observer. Assume also that the antenna firing axis moves parallel to itself.

As the relative positions of the antenna firing axis and the observer change, the angle Υ between Y and Y_0 also changes.

To compute the apparent spin rate of the antenna, mark a reference direction on the plane perpendicular to the firing axis and let P be the time interval between two successive occasions when this direction faces the observer (Fig. 14). If P_0 is the true spin period, then $P = P_0 \pm \Delta t$, where Δt is the time necessary for the antenna to rotate through the angle Υ and the sign depends on the relative motion of the observer and the direction of the spin. Clearly, $\Delta t = (\Upsilon/2\pi)P_0$.

If $d\Upsilon/dt$ is considered constant over one period, then

$$\Upsilon = \frac{d\Upsilon}{dt} P = \frac{d\Upsilon}{dt} P_0 \left(1 \pm \frac{\Upsilon}{2\pi}\right)$$

or

$$\Upsilon = P_0 \frac{d\Upsilon/dt}{1 \mp (P_0/2\pi)(d\Upsilon/dt)}$$

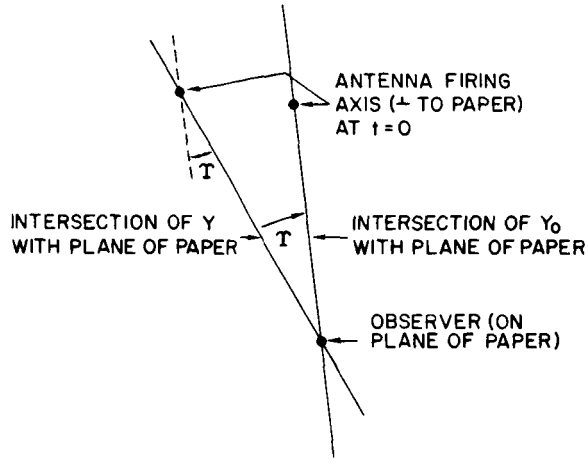

FIG. 14. ANGLES INVOLVED IN CALCULATION OF APPARENT SPIN RATE OF SATELLITE ANTENNA.

and

$$P = \frac{P_0}{1 \mp (P_0/2\pi)(d\Upsilon/dt)} \quad .$$

It now remains to compute $d\Upsilon/dt$ for any given instant of the pass.

For this we will use the topocentric coordinate systems described in Fig. 15. The cartesian axes have the declinations and right ascensions indicated in Figs. 16 and 17.

If $\vec{a}_{OS}$ is the unit vector in the direction from observer to satellite, then the directional cosines will be

$$a_{OS_1} = \cos \epsilon \sin \alpha \tag{5a}$$

$$a_{OS_2} = \cos \epsilon \cos \alpha \tag{5b}$$

$$a_{OS_3} = \sin \epsilon \quad . \tag{5c}$$

Let δ_S be the declination and α_S be the right ascension of the spin axis, and let $\vec{a}_{SS}$ be a vector in the direction of this axis. The

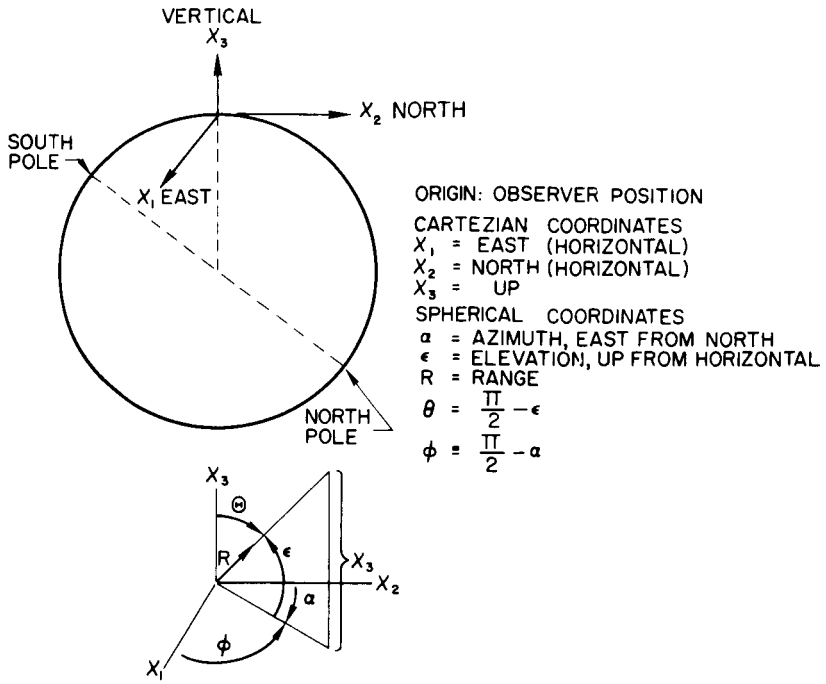

FIG. 15. TOPOCENTRIC COORDINATE SYSTEMS USED AS REFERENCE FOR SPIN AND FARADAY PERIOD COMPUTATIONS.

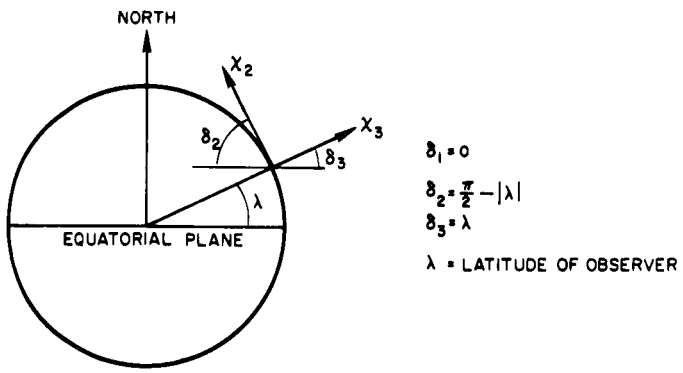

FIG. 16. DECLINATION OF CARTESIAN AXES.

directional cosines with respect to our topocentric cartesian system will be

$$\alpha_{SS_1} = -\cos \delta_S \cos \alpha_S \sin(\ell n - LEQ) + \cos \delta_S \sin \alpha_S \cos(\ell n - LEQ) \quad (6a)$$

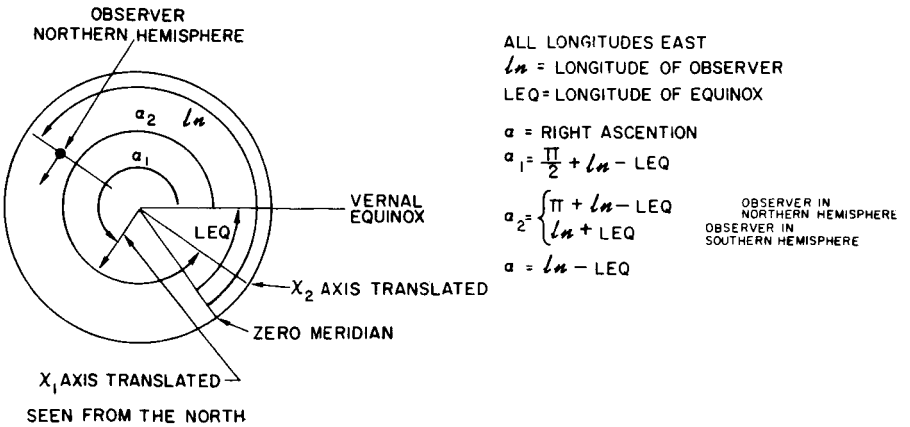

FIG. 17. RIGHT ASCENSION OF CARTESIAN AXES.

$$\alpha_{SS_2} = \mp\cos\delta_S \cos\alpha_S \sin|\lambda| \cos(\ell n\text{-}LEQ) \mp \cos\delta_S \sin\alpha_S \sin|\lambda| \sin(\ell n\text{-}LEQ)$$

$$+ \sin\delta_S \cos\lambda \,, \qquad (6b)$$

where the upper sign corresponds to the Northern Hemisphere, and

$$\alpha_{SS_3} = \cos\delta_S \cos\alpha_S \cos\lambda \cos(\ell n\text{-}LEQ) + \cos\delta_S \sin\alpha_S \cos\lambda \sin(\ell n\text{-}LEQ)$$

$$+ \sin\delta_S \sin\lambda \,. \qquad (6c)$$

The vector

$$\vec{a}_Y \equiv \vec{a}_{OS} \times \vec{a}_{SS} \qquad (7)$$

defines the direction of plane Y at any given moment. Clearly Υ is the angle between $\vec{a}_Y$ and $\vec{a}_{Y_0}$:

$$\cos\Upsilon = \frac{\vec{a}_Y \cdot \vec{a}_{Y_0}}{a_Y \, a_{Y_0}} \,. \qquad (8)$$

Introducing Eq. (5) and (6) into Eq. (7) one can find $\vec{a}_Y$ and, by choosing an arbitrary initial time, can obtain $\vec{a}_{Y_0}$. Consequently, Υ can be found from Eq. (8).

To obtain $d\Upsilon/dt$, Υ is computed at 1-min intervals and successive differences are taken.

Figure 18 shows the theoretically computed curve of apparent spin period (seen from Stanford) vs time for the 2 November 1964 run. The true spin period of 12.024 sec was measured at Goddard Space Flight Center using sun-sensor data. The experimental values follow the general trend of the theoretical curve and there is a good agreement in the absolute values of the spin period after the sharp peak is passed.

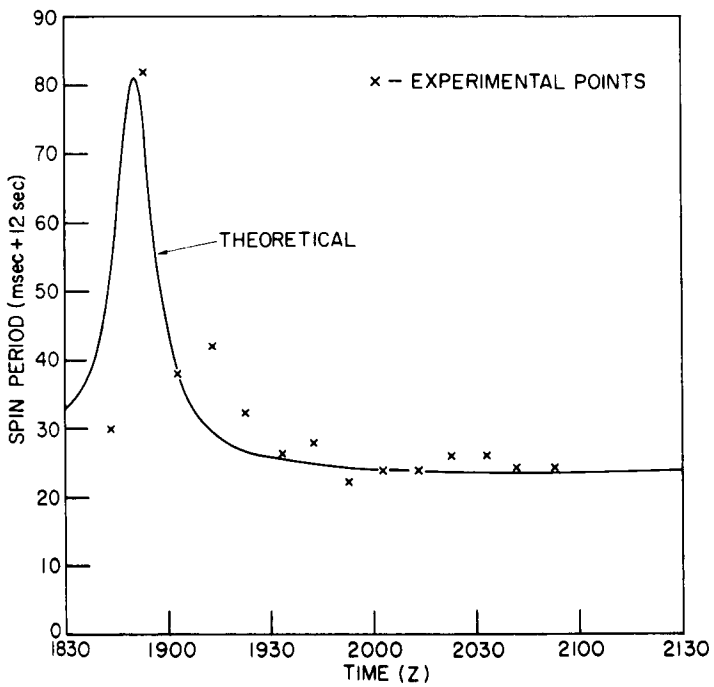

FIG. 18. APPARENT SPIN RATE OF SATELLITE ANTENNA AS SEEN FROM STANFORD.

VI. AZIMUTH CORRECTION FOR RECEIVING ANTENNA

As the receiving antenna swings in azimuth, tracking the satellite, the positions of the Faraday minima change even when there is no modification in the intervening ionization. In vacuum, the minima would occur every time the spinning transmitting antenna appeared to be perpendicular to the direction of the receiving-antenna element.

Let P_1 be a plane defined by the line of sight and the direction of the receiving-antenna element, and P_2 be the plane defined by the same line of sight and the direction of the transmitting-antenna element. As the latter spins, the angle between P_1 and P_2 changes. For any spin-axis direction (except perpendicular to the line of sight), this angle goes through $\pi/2$ twice per rotation. At these points, the vacuum-Faraday signal goes through a null.

We shall adopt the same topocentric coordinate system used in the previous section and define:

$\vec{a}_{OS} \equiv$ unit vector along the line of sight from observer to satellite

$\vec{a}_{SS} \equiv$ unit vector along the spin axis of the satellite antenna

$\vec{a}_{AR} \equiv$ unit vector along the direction of the receiving antenna

$\vec{a}_{AT} \equiv$ unit vector along the direction of the transmitting antenna

$\vec{a}_{P1} \equiv$ unit vector perpendicular to P_1; since $\vec{a}_{AR}$ is perpendicular to $\vec{a}_{OS}$, we define

$$\vec{a}_{P1} \equiv \vec{a}_{AR} \times \vec{a}_{OS} \tag{9}$$

$\vec{a}_{P2} \equiv$ unit vector perpendicular to P_2

$$\vec{a}_{P2} \equiv \vec{a}_{AT} \times \vec{a}_{OS} \, . \tag{10}$$

The directional cosines of $\vec{a}_{OS}$ and $\vec{a}_{SS}$ are given in Chapter V.

We must now determine the components of $\vec{a}_{AR}$ and $\vec{a}_{AT}$ so that $\vec{a}_{P1}$ and $\vec{a}_{P2}$ can be obtained.

Assume that, when the receiving antenna is set at zero elevation, the antenna wire makes an angle γ with the vertical. When the elevation

is increased, the angle β with the vertical changes according to

$$\cos \beta = \cos \gamma \cos \epsilon = a_{AR_3} . \tag{11}$$

Since $\vec{a}_{AR}$ is always perpendicular to the line of sight (i.e., to $\vec{a}_{OS}$):

$$\left(a_{AR_1}\ a_{OS_1}\right) + \left(a_{AR_2}\ a_{OS_2}\right) + \left(a_{AR_3}\ a_{OS_3}\right) = 0 . \tag{12}$$

Finally, a_{AR} is a unit vector and must therefore satisfy

$$a_{AR_1}^2 + a_{AR_2}^2 + a_{AR_3}^2 = 1 . \tag{13}$$

Simultaneous solution of Eqs. (11), (12), and (13) leads to

$$a_{AR_2} = -\cos \alpha \cos \gamma \sin \epsilon \pm \sin \alpha \sin \gamma \tag{14a}$$

$$a_{AR_1} = \frac{\cos^2 \alpha \cos \gamma \sin \epsilon \mp \sin \alpha \cos \alpha \sin \gamma - \cos \gamma \sin \epsilon}{\sin \alpha} . \tag{14b}$$

In the two latter equations we arbitrarily choose the upper sign, thus taking the upward direction of the antenna wire as positive.

The components of $\vec{a}_{Pl}$ can now be written by introducing the values of a_{AR_i} into Eq. (9):

$$a_{Pl_1} = a_{AR_2} a_{OS_3} - a_{AR_3} a_{OS_2} \tag{15a}$$

$$a_{Pl_2} = a_{AR_3} a_{OS_1} - a_{AR_1} a_{OS_3} \tag{15b}$$

$$a_{Pl_3} = a_{AR_1} a_{OS_2} - a_{AR_2} a_{OS_1} . \tag{15c}$$

For the computation of the components of $\vec{a}_{AT}$, we take the direction of the transmitting-antenna wire to be perpendicular to the spin axis. Thus, as the antenna spins around with angular velocity ω_1, its

declination and right ascension vary cyclically: $\sin \delta_A = \cos \delta_S \cos \omega_1 t$, and

$$\alpha_A = \alpha_S - \arccos \left[-\sin \delta_S \frac{\cos \omega_1 t}{(1-\cos^2 \delta_S \cos^2 \omega_1 t)^{1/2}} \right].$$

The first equation is obtained directly from the geometry involved while the second results from constraining the antenna to move perpendicular to the spin axis.

It is now possible to find the directional cosines of $\vec{a}_{AT}$ in the adopted coordinate system:

$$a_{AT_1} = -\cos \delta_A \cos \alpha_A \sin(\ell n\text{-}LEQ) + \cos \delta_A \sin \alpha_A \cos(\ell n\text{-}LEQ) \qquad (16a)$$

$$a_{AT_2} = \mp \cos \delta_A \cos \alpha_A \sin|\lambda| \cos(\ell n\text{-}LEQ)$$

$$\mp \cos \delta_A \sin \alpha_A \sin|\lambda| \sin(\ell n\text{-}LEQ) + \sin \delta_A \cos \lambda \,, \qquad (16b)$$

where the upper sign is for the Northern Hemisphere, and

$$a_{AT_3} = \cos \delta_A \cos \alpha_A \cos \lambda \cos(\ell n\text{-}LEQ)$$

$$+ \cos \delta_A \sin \alpha_A \cos \lambda \sin(\ell n\text{-}LEQ) + \sin \delta_A \sin \lambda \,. \qquad (16c)$$

By introducing Eq. (16) into Eq. (10), we can find the components of $\vec{a}_{P2}$

$$a_{P2_1} = a_{AT_2} a_{OS_3} - a_{AT_3} a_{OS_2} \qquad (17a)$$

$$a_{P2_2} = a_{AT_3} a_{OS_1} - a_{AT_1} a_{OS_3} \qquad (17b)$$

$$a_{P2_3} = a_{AT_1} a_{OS_2} - a_{AT_2} a_{OS_1} \,, \qquad (17c)$$

where the different a_{P2_i} are functions of $\omega_1 t$. We want to find the values of this latter quantity that satisfy the condition for perpendicularity between P_1 and P_2:

$$a_{P1_1} a_{P2_1} + a_{P1_2} a_{P2_2} + a_{P1_3} a_{P2_3} = 0 \ . \qquad (18)$$

To find these values the computer calculates a_{AR_i} and a_{OS_i} for every minute of the pass and, introducing these parameters in Eq. (18), solves for the value of t (nearest the assumed full minute) that satisfies Eq. (18). The time interval between two successive solutions is the duration of 10 semi-revolutions. The "Vacuum Faraday Period," defined as the time interval between the occurrence of two alternate nulls (assuming no ionization change), is then easily found. This Vacuum Faraday Period, used in computing the Faraday-rotation angle as explained in Section VIII.C contains all the necessary corrections for apparent spin rate and receiving-antenna azimuth changes. Figure 19 compares true spin period, apparent spin period (calculated and observed), and the Vacuum Faraday Period.

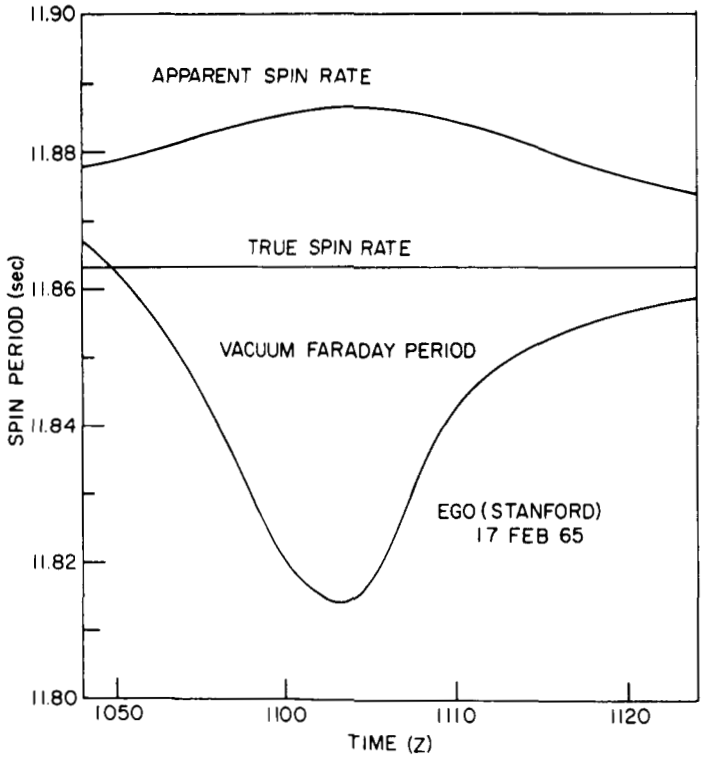

FIG. 19. APPARENT SPIN RATE OF SATELLITE ANTENNA AS SEEN FROM STANFORD.

VII. EFFECTIVE ZENITHAL ANGLE IN THE EXOSPHERE

In Chapter III the columnar electron content of the exosphere up to satellite altitude was defined as the difference between the columnar contents from Doppler and from Faraday measurements. Since we are dealing with slant contents, the number obtained in such a fashion is also the slant content of the exosphere and should be converted to vertical content for proper interpretation. This conversion requires knowledge of the exosphere density profile, which is not known; hence, only a rough approximation can be found, by assuming a plausible model.

Figure 20 shows the pertinent geometry.

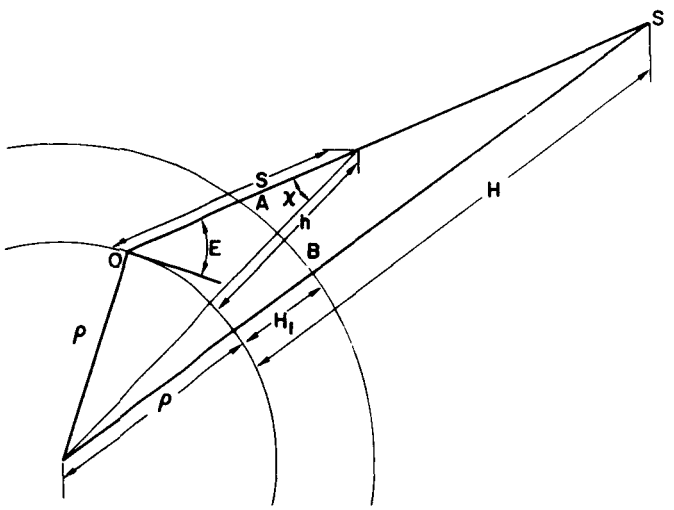

FIG. 20. GEOMETRY NECESSARY FOR ESTIMATION OF EFFECTIVE EXOSPHERE ZENITHAL ANGLE.

$$I_S \equiv \int_A^S N\, ds \qquad \text{(density of column A to S)}$$

$$I \equiv \int_B^S N\, dh \qquad \text{(same as density of columns B to S if perfect stratification exists).}$$

From the geometry,

$$\frac{\sin \chi}{\rho} = \frac{\cos \epsilon}{\rho+h}$$

$$\sin \chi = \frac{\rho}{\rho+h} \cos \epsilon$$

$$\cos \chi = \frac{[(\rho+h)^2 - \rho^2 \cos^2 \epsilon]^{1/2}}{\rho+h}$$

$$ds = \frac{dh}{\cos \chi} .$$

Then

$$I_S = \int_A^S \frac{N(h)}{\cos \chi} dh = \int_A^S \frac{N(h) \times (\rho+h)\, dh}{[(\rho+h)^2 - \rho^2 \cos^2 \epsilon]^{1/2}} = \int_A^S \frac{N(r) r dr}{[r^2 - a^2]^{1/2}}$$

where $r \equiv \rho+h$ and $a \equiv \rho \cos \epsilon$.

We want $\sec \chi_{eff} \equiv I_S/I$, and to find it we must assume an exosphere profile. The model that best fits the meager data available is based on a $1/r^3$ law.

Let $N = N_0(r_0/r)^3$ for $r > r_0 = \rho+H_1$. Then

$$I_S = N_0 r_0^3 \int_{r_0}^{r} \frac{dr}{r^2(r^2-a^2)^{1/2}} = N_0 r_0^3 \left. \frac{(r^2-a^2)^{1/2}}{a^2 r} \right|_{r_0}^{r}$$

$$= \frac{N_0 r_0^3}{a^2} \left[\left(1 - \frac{a^2}{r^2}\right)^{1/2} - \left(1 - \frac{a^2}{r_0^2}\right)^{1/2} \right],$$

and $I = I_S(\epsilon = \pi/2)$.

Since $a \to 0$ when $\epsilon \to \pi/2$ the above expression for I_S becomes indeterminate for vertical incidence. To lift the indeterminancy we expand the square root:

$$I_S = \frac{N_0 r_0^3}{a^2}\left[1 - \frac{a^2}{2r^2} - \frac{a^4}{8r^4} - \frac{a^6}{16r^6} - \cdots - 1 + \frac{a^2}{2r_0^2} + \frac{a^4}{8r_0^4} + \frac{a^6}{16r_0^6} + \cdots\right]$$

$$= \frac{N_0 r_0^3}{2}\left[\left(\frac{1}{r_0^2} - \frac{1}{r^2}\right) + \frac{a^2}{4}\left(\frac{1}{r_0^4} - \frac{1}{r^4}\right) + \frac{a^4}{8}\left(\frac{1}{r_0^6} - \frac{1}{r^6}\right) + \cdots\right]$$

and, when $\epsilon = \pi/2$,

$$I = \frac{N_0 r_0^3}{2}\left(\frac{1}{r_0^2} - \frac{1}{r^2}\right).$$

Hence

$$\sec \chi_{eff} = 2\,\frac{\left|1 - [(\rho/r)\cos\epsilon]^2\right|^{1/2} - \left|1 - [(\rho/r_0)\cos\epsilon]^2\right|^{1/2}}{(\rho\cos\epsilon)^2\,[(1/r_0^2) - (1/r^2)]} \qquad (19)$$

This equation allows us to convert from the measured slant-columnar content of the exosphere into a first approximation of what may be called the vertical-columnar content of that region.

VIII. FIRST-ORDER ANALYSIS

A. DIFFERENTIAL-DOPPLER-FREQUENCY METHOD

The methods for calculating the columnar electron content of the ionosphere by the differential-Doppler-frequency technique have been fully described by many authors, as, for instance, Ross [1960] and de Mendonca [1962]. A recapitulation is presented here for sake of completeness.

Let ϕ be the phase of a signal radiated from a transmitter.

If the radiated frequency ω is constant, and a path of length R, in vacuum, separates transmitter from receiver, then the phase at the latter will be $\phi_r = \omega t - (2\pi R/\lambda)$ where λ is the wavelength.

However, if there is intervening ionization, λ will vary along the path and

$$\phi_r = \omega t - 2\pi \int_0^R \frac{ds}{\lambda(s)} = \omega t - 2\pi \int_0^R \frac{f}{v_p}\, ds$$

$$= \omega t - \frac{\omega}{c} \int_0^R \mu(s) ds \ .$$

The angular frequency at the receiver is:

$$\omega_r = \frac{d\phi_r}{dt} = \omega - \frac{\omega}{c} \frac{d}{dt} \int_0^R \mu(s)\, ds \ .$$

If two coherent frequencies, ω_1 and $\omega_2 = n\omega_1$, are transmitted,

$$\omega_{r_1} = \omega_1 - \frac{\omega_1}{c} \frac{d}{dt} \int_0^R \mu_1(s)\, ds$$

and

$$\omega_{r_2} = n\omega_1 - \frac{n\omega_1}{c} \frac{d}{dt} \int_0^R \mu_2(s)\, ds \ .$$

When the higher received frequency is divided by n and the result is subtracted from the lower received frequency, a slowly varying beat-note ω_D, called the differential-Doppler angular frequency, is obtained.

$$\omega_D \equiv \omega_{r_1} - \frac{\omega_{r_2}}{n} = \frac{\omega_1}{c} \frac{d}{dt} \int_0^R \mu_2(s)\, ds - \int_0^R \mu_1(s)\, ds \ . \tag{20}$$

Since the refractive index is frequency-dependent, $\mu_1 \neq \mu_2$. Also, notwithstanding the fact that the integration paths have common terminal points (the transmitter and receiver), they do differ by virtue of the dissimilar refraction of the two signals (Fig. 21).

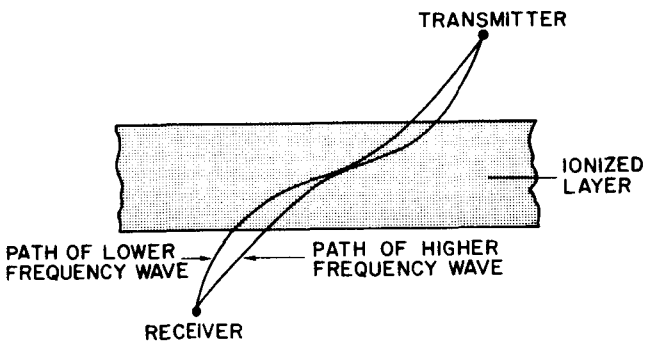

FIG. 21. REFRACTION EFFECT ON THE PATHS OF WAVES OF DIFFERENT FREQUENCIES THROUGH AN IONIZED LAYER.

Approximation I. Assume similar paths.

Under the simplifying Approximation I, Eq. (20) reduces to

$$\omega_D = \frac{\omega_1}{c} \frac{d}{dt} \int_0^R [\mu_2(s) - \mu_1(s)]\, ds \ . \tag{21}$$

Approximation II. Assume there is no steady magnetic field.

Approximation III. Assume no collisions.

With Approximations II and III, the refractive index can be expressed as

$$\mu^2 = 1 - \frac{\omega_p^2}{\omega^2} = 1 - \frac{K_D N(s)}{f^2} \quad ,$$

where $N(s)$ is the electron density and $f = \omega/2\pi$, and

$$K_D = \frac{e^2}{4\pi^2 m \epsilon_0} = 80.62 \ m^3/sec^2 \ .$$

Approximation IV. Assume the received frequencies are much larger than the plasma frequency--$\omega^2 \gg \omega_p^2$.

We can then write

$$\mu = 1 - \frac{K_D N(s)}{2f^2} \ . \tag{22}$$

Equation (21) reduces to

$$f_D = \frac{K_D}{2cf} \left(\frac{n^2-1}{n^2} \right) \frac{d}{dt} \int_0^R N(s) \, ds$$

$$= Q \frac{d}{dt} \int_0^R N(s) \, ds \ , \tag{23}$$

where $Q = 3.31 \times 10^{-15}$ for $f_1 = 40$ Mc and $f_2 = 360$ Mc.

From Eq. (23),

$$\frac{1}{Q} \int_0^t f_D \, dt + I_{SD_0} = \int_0^R N(s) \, ds = I_{SD} \ . \tag{24}$$

The slant-columnar electron content I_{SD} from ground to satellite is given, for any moment, by Eq. (24), provided we know the total content I_{SD_0}, at time $t = 0$, which must be found by independent means. In the EGO experiment it is derived from group-delay measurements. $\int_0^t f_D \, dt$ is simply the differential-Doppler cycle count. To obtain this from the EGO records, the effect of satellite spin must be taken into account. As we showed in Chapter IV the spinning of the satellite introduces an additional differential-Doppler frequency so that

$$f_D = f_d - \frac{10}{9} f_r ,$$

where f_d is the recorded frequency and f_r is the spin frequency.

B. GROUP-DELAY METHOD

This method of measuring the columnar ionization content between ground and satellite is used to provide an absolute reference value for the integration of the differential-Doppler-frequency data. The results of the group-delay method itself cannot conveniently be used in the final analysis (thereby dispensing with Doppler) because of the larger spread of the data points and by virtue of the fact that much better signal-to-noise ratios are required, rendering it impossible to obtain this kind of information except when the satellite is at relatively short range.

The method consists of comparing the phase of arrival of the modulation envelopes of the 40- and 360-Mc signals. This phase depends on the relative group velocity of the two frequencies and, therefore, on the ionization traversed.

Equation (22) gave us a simplified expression for the refractive index and since, under the assumption of no collison, the group velocity is $V_g = c\mu$, this velocity can be expressed as

$$V_g = c\left(1 - \frac{K_D N}{2f^2}\right) \approx \frac{c}{1 + (K_D/2f^2)N} .$$

Let t be the time for a signal to travel between satellite and observer:

$$t = \int_0^R \frac{ds}{V_g} = \frac{1}{c} \int_0^R \left(1 + \frac{K_D}{2f^2} N\right) ds$$

$$= \frac{R}{c} + \frac{K_D}{2cf^2} I_s \ .$$

At a frequency n times higher, the time will be

$$t_n = \frac{R_n}{c} + \frac{K_D}{2cn^2f^2} I_{s_n} \ .$$

In general, as a result of the different paths taken by the signals at different frequencies, $R_n \neq R$ and $I_{s_n} \neq I_s$.

Approximation I. Assume similar paths.

Then

$$\Delta t \equiv t - t_n = \frac{K_D}{2cf^2} I_s \left(1 - \frac{1}{n^2}\right)$$

$$= \frac{K_D}{2cf^2} \frac{n^2-1}{n^2} I_s \ . \qquad (25)$$

If both carriers are modulated (in the same phase) by a frequency f_M, the retardation Δt will reveal itself as a phase difference $\Delta\phi$ between the two demodulated tones,

$$\Delta\phi = 2\pi f_M \Delta t \ . \qquad (26)$$

Combining Eqs. (25) and (26) and solving for I_s gives

$$I_s = \frac{c}{\pi K_D} \frac{n^2}{n^2-1} \frac{f^2}{f_M} \Delta\phi \ .$$

For the values used in EGO,

$$f = 40.01 \text{ Mc}$$

$$f_M = 0.2 \text{ Mc}$$

$$n = 9,$$

and, expressing $\Delta\phi$ in degrees,

$$I_s = 1.673 \times 10^{14} \times \Delta\phi \text{ electrons/m}^2 .$$

C. FARADAY-ROTATION-ANGLE METHOD

This method of measuring the total electron content of the ionosphere has received wide attention mainly because of the simplicity of the equipment necessary. This equipment may be a common communications receiver, in contrast with the differential-Doppler-frequency method that requires, generally, the use of phase-lock receivers.

A good description of the theory behind the measurements can be found in an article by Garriott [1960].

The anisotropic nature of the ionosphere, due to the presence of a steady geomagnetic field, results in the splitting of the high-frequency electromagnetic wave into two components; associated to each one is a different refractive index.

Approximation III. Assume no collisions.

The Appleton-Hartree equation for the refractive index reduces to

$$\mu^2 = 1 - X \left\{ 1 - \frac{Y_T^2/2}{1 - X} \pm \left[\frac{Y_T^4/4}{(1-X)^2} + Y_L^2 \right]^{1/2} \right\}^{-1} .$$

Approximation V. Assume quasi-longitudinal conditions [Ratcliff, 1962, Chapter 8].

Then

$$\mu^2 = 1 - \frac{X}{1 \pm |Y_L|} . \qquad (27)$$

Approximation IV. Assume $\omega^2 \gg \omega_p^2$. $\therefore$ $X \ll 1$.

Approximation VI. Assume $\omega \gg \omega_g$. $\therefore$ $Y_L \ll 1$.

Applying these approximations, Eq. (27) can be written

$$\mu = 1 - \frac{X}{2} (1 \mp |Y_L|) ,$$

which gives a simplified expression for the indexes of refraction corresponding to the two magnetoionic modes, each of which is circularly polarized, one right-handed and one left-handed. The difference between the two values of μ causes the phase-path length of the two modes to be unequal, so that the resulting wave is linearly polarized, with a polarization plane that slowly rotates as the signal propagates through the medium.

The phase-path lengths are

$$P_u = \int_0^R \mu_u \, ds$$

and

$$P_l = \int_0^R \mu_l \, ds .$$

If we make Approximation I assuming identical paths, then the phase-path difference is

$$\Delta P = \int_0^R (\mu_u - \mu_l) \, ds = \int_0^R XY_L \, ds ,$$

which corresponds to a rotation angle

$$\Omega = \pi \frac{\Delta P}{\lambda} = \frac{\pi f}{c} \int_0^R XY_L \, ds \ .$$

Approximation VII. Represent the effect of the Y_L factor inside the integral by an average $\overline{Y_L}$:

$$\Omega = \frac{\pi f}{c} \overline{Y_L} \int_0^R X \, ds$$

or

$$\Omega = \frac{\mu_0 e^3}{8\pi^2 c \epsilon_0 m^2} \frac{H \cos \theta}{f^2} I_S$$

$$= \frac{K_F}{f^2} G I_S \ ,$$

where:

$$K_F \equiv \frac{\mu_0 e^3}{8\pi^2 c \epsilon_0 m^2} = 0.02976 \ (\text{mks})$$

$$G \equiv \overline{H \cos \theta} \ .$$

G is evaluated at the "ionosphere point," defined as the intersection of the line of sight from observer to satellite with a spherical shell at an altitude conveniently chosen. The value of H is obtained from an expansion of the geomagnetic field in six spherical harmonics as described by Eckhouse [1964].

The total rotation angle is usually of the order of many tens of radians, while experimentally the measurements yield values between 0 and π leaving an $n\pi$ ambiguity. It is therefore necessary to determine, by independent means, the value of I_S at one given time of a run. The value of I_S at any other time can then be computed from the experimental data.

For the EGO experiment, differential-Faraday-rotation-angle measurements are used to establish this reference so that, at $t = t_0$,

$$\Omega(t_0) = \frac{K_F}{f^2} G(t_0)\ I_S(t_0)$$

and at any other time

$$I_S(t) = \frac{1}{G(t)} \left[G(t_0)\ I_S(t_0) + \frac{f^2}{K_F} \Delta\Omega \right] ,$$

where $\Delta\Omega \equiv \Omega(t)-\Omega(t_0)$ is obtained from the experiment as described below.

The Faraday minima are numbered consecutively and a tabulation is made of the time of occurrence of every tenth minimum (to the nearest 0.1 sec). They repeat approximately every half satellite-spin period. Assume that the reference value for the total slant electron content was obtained at the occasion of the n_r minimum (at time t_{n_r}). If Ω did not change, then the next minimum would occur at

$$t = t_{n_r} + \frac{P}{2} \left(t_{n_r} \right) .$$

However, if $\Delta\Omega \neq 0$, then $t \neq t_{n_{r+1}}$ and

$$\Delta\Omega = 2\pi \frac{t - t_{n_{r+1}}}{P\left(t_{n_r+1} \right)} = \frac{2\pi}{P\left(t_{n_{r+1}} \right)} \left[\frac{1}{2} P\left(t_{n_{r+1}} \right) + t_{n_r} - t_{n_{r+1}} \right] .$$

It should be pointed out here that, as discussed in Chapter V on spin-period error, P, the vacuum Faraday period, is not constant, but rather a function of time.

If the next tabulated minimum after n_r is n_{r+1} (do not confuse n_r+1 with n_{r+1}), then

$$\Omega\left(t_{n_{r+1}} \right) - \Omega\left(t_{n_r} \right) = \frac{2\pi}{P\left(t_{n_{r+1}} \right)} \left[(n_{r+1} - n) \frac{1}{2} P\left(t_{n_{r+1}} \right) + t_{n_r} - t_{n_{r+1}} \right]$$

and, in general,

$$\Omega\left(t_{n_{r+m}}\right) - \Omega\left(t_{n_r}\right) = \frac{2\pi}{P\left(t_{n_{r+m}}\right)} \left[\left\{\sum_{i=0}^{m} \left(n_{r+i+1} - n_{r+i}\right) \frac{P}{2} \left(t_{n_{r+i+1}}\right)\right\} + t_{n_r} - t_{n_{r+m}}\right] . \qquad (28)$$

A similar expression can be developed for the minima that precede n_r.

D. DIFFERENTIAL-FARADAY-ROTATION-ANGLE METHOD

It was pointed out in the previous chapter that it is necessary, in order to use the Faraday-rotation-angle data, to obtain one reference value for the total slant content from an independent measurement. The differential Faraday technique was adopted to this end for the EGO experiment.

The beacon transmitters aboard the satellite are phase modulated by a 200-kc tone in such a way that the sidebands and carrier have approximately the same power. In effect, if f_0 is the carrier frequency, we have three signals of frequencies (in megacycles)

$$f_- = f_0 - 0.2$$

$$f_0$$

$$f_+ = f_0 + 0.2 .$$

The Faraday rotation observed on the ground will differ slightly for each signal. Let us take the f_- and f_+ pair. The difference in Faraday rotation will be

$$\Delta\Omega = K_F \, GI_S \left(\frac{1}{f_-^2} - \frac{1}{f_+^2}\right) .$$

For all realistic conditions $\Delta\Omega$ will be smaller than π radians and there is no ambiguity in the measurement. The angle $\Delta\Omega$ is scaled directly from the Faraday fading record, but a rather wide scatter is observed, requiring the averaging of many measurements to obtain a reliable value of I_S.

IX. ERRORS

Because the final result of the data-reduction process in the EGO experiment is the difference between the columnar contents derived by two methods, and since this is a small difference between large numbers, it is important to examine the effect of all approximations made in the first-order analysis, described in the preceding chapters, and to introduce corrections whenever the error is of a magnitude comparable with the desired output. In addition, other sources of error must be sought out and, if necessary, corrected.

The main uncertainties in the results stem from the following origins.

1. Errors due to the uncertainty in the spin rate
2. Errors due to the uncertainty in the satellite position
3. Errors due to the inaccuracy in absolute reference value of columnar electron content
4. Errors due to the uncertainties in data scaling.

In the next two sections, we analyze the effect of choosing a wrong value for the spin rate of the satellite in the reduction of both differential-Doppler-frequency and Faraday-rotation-angle data.

It is shown that, whereas the Doppler method is relatively insensitive to small spin-rate errors, the Faraday results depend critically on these values. Precision of the order of ±1 msec in the roughly 12-sec spin period is desirable. This accuracy can be obtained from solar-sensor data, and the Goddard Space Flight Center (GSFC) has provided the necessary information for some of the runs. It is also, in some occasions, possible to derive the spin period to nearly the above tolerance from the observation of the amplitude fades of the 360-Mc signal received with a circular antenna.

A. SPIN-RATE ERROR IN DIFFERENTIAL-DOPPLER-FREQUENCY METHOD

In Section VII.A, the slant-columnar content from differential-Doppler-frequency data is given by

$$I_{SD} = I_{SD_0} + \frac{1}{Q} \int_0^t (f_d - af_r)\, dt \ ,$$

where $a = (9\pm1)/9$ depending on the relative polarization of the 40- and 360-Mc receiving antenna, and f_r is the spin frequency of the probe.

If we assume that both f_d and f_r are constant,

$$I_{SD} = I_{SD_0} + \frac{1}{Q}(f_d - af_r)t$$

and

$$\frac{dI_{SD}}{df_r} = -\frac{at}{Q} .$$

This statement means that an error of Δf will result in an error ΔI_{SD} that is proportional to the time:

$$\Delta I_{SD} = -\frac{a}{Q}\Delta f_r \, t .$$

For example, let the true spin period be 12.025 sec and assume that a +5-msec error was made in the estimation of this period. The true spin frequency would be 0.0831 cps and the error would be $\Delta f_r = -3.455 \times 10^{-5}$ cps. With $a = 10/9$ the error after one hour would be about 4×10^{13} electrons/m^2. If in this hour the satellite rose 15,000 km (say, from 10,000 to 25,000 km) this change would result in an error of 2.7 electrons/m^3 in the estimation of the average exosphere electron density.

As shown below, this error is negligible compared with the one introduced by a similar spin-period uncertainty in the Faraday measurement.

B. SPIN-PERIOD ERROR IN FARADAY-ROTATION-ANGLE METHOD

As shown in Section VIII.C, the change in Faraday rotation from a given arbitrary reference value Ω_0 is

$$\Omega_{r+n} - \Omega_0 = \frac{2\pi}{P(t_{r+n})}\left[\left\{\sum_{i=0}^{n}(n_{r+i+1} - n_{r+i})\frac{P(t_{r+i+1})}{2}\right\} + t_r - t_{r+n}\right] .$$

To estimate the error introduced by an incorrect value of P, let us assume that both the incorrect and correct values are time-independent. This assumption simplifies the above equation to

$$\Omega_{r+n} - \Omega_0 = \pi\left[n_{r+n} - n_r + \frac{2}{P}(t_r - t_{r+n})\right]$$

and

$$\frac{d(\Omega_{r+n} - \Omega_0)}{dP} = -\frac{2\pi}{P^2}(t_r - t_{r+n}) .$$

Thus, if P = 12 sec and dP = ΔP = 0.005 sec,

$$\Delta(\Omega_{r+n} - \Omega_0) = 2.2 \times 10^{-4}\, \Delta t .$$

After one hour the error in the Faraday angle will be 0.8 radian or some 45 deg. A typical value for G at Stanford is 25 amp/m. Consequently, the 0.8-radian error will lead to an over- (or under-) estimation of the total content by about 0.17×10^{16} electrons/m^2, a discrepancy some 40 times larger than that found for the Doppler method. Again, assuming that during the above hour the satellite rose 15,000 km, the error in the determination of the average exosphere density would be 110 electrons/m^3, which is comparable to the expected local density. For the above reason, the ±1-msec tolerance was set as a goal for the data interpretation. This tolerance would then leave, under the conditions described, an uncertainty of 22 electrons/m^3 in this example.

C. ERRORS DUE TO UNCERTAINTY IN SATELLITE POSITION

Since the apparent spin rate near perigee is dependent on the position of the satellite, and in view of the fact that this spin rate influences the final result, it is clear that uncertainties in the satellite's location may introduce important errors in the reduced information, especially near the beginning of each run. In order to calculate the factor G in the Faraday-rotation-angle method, and the refraction and zenithal angle corrections, it is also necessary to know the satellite's

position. Predictions of satellite latitude, longitude, and height, whether obtained from GSFC or locally generated, are frequently not accurate enough because of the strong perturbations in the highly eccentric EGO orbit. The shape and position of the orbit are generally known within an adequate tolerance, but the timing may be off by several minutes on occasions. For this reason it proves essential to use a posteriori positions, hopefully correct within 1 min of time.

D. ERROR DUE TO INACCURACY IN REFERENCE VALUE OF COLUMNAR ELECTRON CONTENT IN FARADAY-ROTATION-ANGLE METHOD

The total slant electron content derived from Faraday-rotation-angle data is

$$I_S = \frac{G_0}{G(t)} I_{S_0} + g(t) \qquad (29)$$

where both $g(t)$ and $G(t)$ are functions of time but not of I_{S_0}.

When an incorrect value of I_{S_0} is used, not only is the value of I_S shifted correspondingly but, in addition, a spurious slope in the I_S-vs-t curve is introduced as a result of the larger or smaller weight given the first term on the right-hand side of Eq. (29). This leads to an error in the estimation of the average exosphere density. The magnitude of this spurious slope is assessed below.

Let the correct value of I_S be I_{S_1} and the faulty one I_{S_2}. At time $t = t_0$ the error will be $(I_{S_1}-I_{S_2})_{t_0}$ and, at $t = t_1$, $(I_{S_1}-I_{S_2})_{t_1}$.

Referring to Fig. 21 we see that, in the time interval between t_1 and t_2, the ordinate of the curve with the faulty reference departs from that of the correct one by

$$\Delta I \equiv \left(I_{S_1} - I_{S_2}\right)_{t_1} = \left(I_{S_1} - I_{S_2}\right)_{t_2}$$

$$= \frac{G_0}{G(t_1)} I_{S_{0_1}} - \frac{G_0}{G(t_1)} I_{S_{0_2}} - \frac{G_0}{G(t_2)} I_{S_{0_1}} + \frac{G_0}{G(t_2)} I_{S_{0_2}}$$

$$= G_0 \left(I_{S_{0_1}} - I_{S_{0_2}}\right) \left[\frac{1}{G(t_1)} - \frac{1}{G(t_2)}\right].$$

As an example, consider the following values obtained during the 2 November 1964 pass of EGO, at Stanford.

Time (Z)	Height (km)	G amp/m
18:49	10,000	30.35
19:49	25,300	24.94

Reference value (assumed correct) $I_{S_{0_1}} = 16.8 \times 10^{16}$ electrons/m^2 at 19:31Z, $G_0 = 25.33$ amp/m.

Assume a 10-percent error in the above reference value, so that

$$I_{S_{0_2}} = 15.1 \times 10^{16} \text{ electrons/m}^2$$

and

$$\Delta I = 0.31 \times 10^{16} \text{ electrons/m}^2 .$$

These values would correspond, under the conditions of the example used in the preceding sections, to an erroneous estimate of the average exosphere electron density equal to 207 electrons/m^3. This would certainly obscure the true value to be measured. One must conclude that, in this particular case, in order to reduce the uncertainty caused by the use of incorrect reference value to some 20 electrons/m^3, the reference should have a tolerance of about 1 percent. However, this is an unattainable accuracy in this kind of measurement.

It is therefore clear that one can hope only to obtain a good estimate of local electron densities in the neighborhood of regions where the tangential motion of the satellite, as seen from the ground, is very small, resulting in only minor changes in G. The above discussion indicates that the greatest effort should be made in the direction of obtaining the best possible value from the differential-Faraday-rotation-angle method.

X. SECOND-ORDER ANALYSIS

The approximations in the first-order analysis were:

I Similar raypaths are assumed for both higher- and lower-frequency waves in the differential-Doppler-frequency and group-delay measurements.

II In the differential-Doppler-frequency and group-delay measurements, it is assumed that there is no geomagnetic field.

III In all measurements it is assumed that there are no collisions.

IV It is assumed that all operating frequencies are much higher than the plasma frequency.

V Quasi-longitudinal propagation conditions are assumed.

VI It is assumed that the frequencies at which Faraday rotation is being observed are much higher than the maximum electron gyro-frequency.

VII The effect of the gyro-frequency is represented by an average value calculated at the height of the ionosphere point.

Approximation III is good under all conditions, while V is good under all conditions for the stations involved in this project since the satellite, as a result of its low inclination, is never seen toward the north.

The refraction and path-splitting effects implicitly ignored through Approximation I and the linearization of the refractive index as a function of electron density and magnetic field, made by Approximations IV and VI respectively, will be all taken into account by means of equations derived by Ross [1965], as will be the effect of the geomagnetic field on the differential-Doppler measurements (Approximation II).

A. DIFFERENTIAL-DOPPLER-FREQUENCY METHOD

For the case of a radio source well above the bulk of the ionization, Ross [1965] has shown that the phase-path defect, corrected for second-order effects, is given by

$$\Delta P = (h\bar{X}/2) \sec \chi (1 \mp Y_L + (\beta\bar{X}/4) \bar{X} \sec^2 \chi)$$

where $\bar{X} \equiv \left(\int_0^h X dh\right)/h$ is the height average of X

$\beta \equiv \overline{X^2}/\bar{X}^2$ is a factor related to the nonuniformity of the ionization distribution with height.

For a uniform slab of ionization of width d, $\beta = h/d$ and for a Chapman layer of scale height H, $\beta = 0.16h/H$;

$$h\bar{X} \sec \chi = \frac{K_D}{f^2} I_S \tag{30}$$

$$\beta\bar{X} = \frac{\Lambda K_D}{f^2} I \ , \tag{31}$$

which is seen to be height-independent.

For slab, $\Lambda = \frac{1}{d}$

For Chapman, $\Lambda = \frac{0.16}{H}$.

Thus

$$\Delta P = \frac{K_D I_S}{2f^2}\left[1 \mp Y_L + \frac{\Lambda}{4}\frac{K_D}{f^2} I_S \sec \chi\right] . \tag{32}$$

The Y_L term provides the geomagnetic correction, while the last term inside the brackets originates in part from refraction effects and in part from the nonlinearity of the refractive index with electron density.

$$f_{D_1} = \frac{f}{c}\dot{\Delta P} = \frac{K_D}{2cf}\left[\frac{d}{dt} I_S \mp \frac{d}{dt}(I_S Y_L) + \frac{\Lambda}{4}\frac{K_D}{f^2}\frac{d}{dt}\left(I_S^2 \sec \chi\right)\right] . \tag{33}$$

At a frequency n times higher,

$$f_{D_2} = \frac{K_D}{2cfn}\left[\frac{d}{dt} I_S \mp \frac{1}{n}\frac{d}{dt}(I_S Y_L) + \frac{\Lambda}{4}\frac{K_D}{n^2 f^2}\frac{d}{dt}(I_S^2 \sec x)\right],$$

but the two last terms are second-order corrections; if n is sufficiently high they become negligible:

$$f_{D_2} = \frac{K_D}{2cfn}\frac{d}{dt} I_S \tag{34}$$

$$f_D \equiv f_{D_1} - \frac{1}{n} f_{D_2} = \frac{K_D}{2cf}\left[\left(1 - \frac{1}{n^2}\right)\frac{d}{dt} I_S \mp \frac{d}{dt}(I_S Y_L) + \frac{\Lambda}{4}\frac{K_D}{f^2}\frac{d}{dt}(I_S^2 \sec x)\right]$$

$$= \int_0^t f_D \, dt + Q\, I_{SD_0}$$

$$= \frac{K_D}{2cf}\left(1 - \frac{1}{n^2}\right) I_S \mp \frac{K_D}{2cf} I_S Y_L + \frac{\Lambda}{8c}\frac{K_D^2}{f^3} I_S^2 \sec x$$

$$\equiv Q\, I_S', \tag{35}$$

where I_S' is the value of total content obtained from the first-order analysis.

Equation (34) is quadratic in I_S and can be solved directly, yielding

$$I_S = \frac{\{[n^2/(n^2-1]Y_L - 1\} + \{(1 \mp [n^2 Y_L/(n^2-1)])^2 + I_S'(\Lambda K_D/f^2) \sec x\}^{\frac{1}{2}}}{(\Lambda K_D/2f^2) \sec x} \tag{36}$$

where the + sign was taken in front of the square root, so that Eq. (36) reduces to the first-order solution, when the coefficient of I_S^2 tends toward zero, or I_S' can be computed initially and a correction can be applied, as shown below.

$$I_S = \frac{I_S'}{1 \mp [n^2/(n^2-1)]Y_L + (AK_D/4f^2)I_S' \sec \chi} \quad . \tag{37}$$

The choice of signs in Eqs. (32) through (37) depends on which of the two magnetoionic modes is received.

In the Northern Hemisphere, a downward propagating wave with right-circular (clockwise) polarization is the extraordinary component. Hence a circularly polarized ground receiving antenna pointing upward to a satellite will, in general, select the ordinary mode (upper sign in our equations) if it is left-circular (counterclockwise) and vice-versa.

We see that a left-circular antenna in the Northern Hemisphere, imposing the use of a negative signal in Eq. (32), causes a partial cancellation of the geomagnetic correction by the third term in the bracket. The use of such an antenna thus minimizes the second-order corrections for differential-Doppler measurements.

B. FARADAY-ROTATION-ANGLE METHOD

Again referring to Ross' paper [1965] we find that, if Ω' is the first-order approximation of the Faraday rotation angle, then the second-order angle Ω is given by

$$\Omega = \Omega'\left[1 + \frac{\beta\bar{X}}{2} + \frac{\beta-1}{2} J \bar{X}\right] .$$

Here J is a geometrical factor defined by

$$J = \tan \chi(\tan \chi - \tan \theta)$$

and χ and θ have the same meaning as in Sec. VII.C.

If the source is well above most ionization, $\beta \gg 1$ and, by using Eq. (31), we get

$$\Omega = \Omega' \left[1 + \frac{\Delta K_D}{2f^2} I_S (1 + J) \right] .$$

Since $\Omega' = (K_F G / f^2) I_S$, we can find a quadratic for I_S:

$$\frac{\Delta K_D K_F G (1+J)}{2f^4} I_S^2 + \frac{K_F G}{f^2} I_S - \Omega = 0 ,$$

which may be solved directly or through the same process of iteration used in the last section, yielding

$$I_S = \frac{I_S'}{1 + \{ [\Delta K_D (HJ) I_S'] / 2f^2 \}} .$$

In view of the relatively high frequency used (40 Mc) the second-order corrections discussed in this chapter are relatively small.

Using the more favorable antenna polarization, left-circular, alluded to in Chapter V, we find the values of the corrections are, typically, as shown below:

Elevation (deg)	Second-order for Faraday (percent)	Correction for Doppler (percent)
12	-1.5	-6.3
20	-1.9	-3.5
40	-0.5	-2.1
70	-0.1	-1.3

If a right-circular antenna is used, the corrections for Doppler are roughly doubled while those for Faraday remain unchanged. It should be pointed out that these corrections are azimuth-dependent, as a result of the geomagnetic-field influence.

BIBLIOGRAPHY

Eckhouse, Jr., Richard H., Report, Electrical Engineering Research Laboratory, University of Illinois, 1964.

Garriott, O. K., "The Determination of Ionospheric Electron Content and Distribution from Satellite Observations. Part 1. Theory of the Analysis," J. Geophys. Res., 65, 1960, p. 1139.

Garriott, O. K., F. L. Smith, and P. C. Yuen, "Observations of Ionospheric Electron Content Using a Geostationary Satellite," Preprint, Radioscience Laboratory, Stanford University, 1965.

de Mendonca, F., "Ionospheric Electron Content and Variations Measured by Doppler Shifts in Satellite Transmissions," J. Geophys. Res., 67, 1962, p. 2315.

Ratcliff, J. A., The Magneto-Ionic Theory and Its Applications to the Ionosphere, Cambridge University Press, Cambridge, 1962.

Ross, W. J., "Determination of Ionosphere Electron Content from Satellite Doppler Measurements," J. Geophys. Res., 65, 1960, p. 2601.

Ross, W. J., "Second-Order Effects in High-Frequency Transionospheric Propagation," J. Geophys. Res., 70, 1965, p. 597.

Stanford Electronics Laboratories
Technical Report No. 1
National Aeronautics and Space Administration

"Eccentric Geophysical-Observatory Satellite S-49 with Interpretation of the Radio-Beacon Experiment" A. V. da Rosa SEL-65-063

ERRATA

Page	
7	Caption of Figure 4 should read: "Sunset and sunrise effects are clearly visible in the beginning of the vertical-content curves in a. and in the end in c., respectively."
8	The following sentence should be added to the caption on Figure 5: "The difference has been converted to 'vertical columnar content' as explained in Section VII."
45 and 47	The electron concentrations in the examples are per cubic centimeter and not per cubic meter as indicated.
46	The reference to Figure 21 should be ommitted.